Magnetoelectric and second-harmonic spectra in antiferromagnetic Cr_2O_3

Makiko Muto, Yukito Tanabe, Takako Iizuka-Sakano, and Eiichi Hanamura
Department of Applied Physics, University of Tokyo, 7-3-1 Hongo, Bunkyo-ku, Tokyo 113, Japan
(Received 9 April 1997; revised manuscript received 20 October 1997)

We present a microscopic model to understand the magnetoelectric and second-harmonic spectra of Cr_2O_3 and the interference effect between the magnetic (χ^m) and electric (χ^e) second-order optical polarizations. The spin-orbit interaction and the crystalline fields of correct symmetry around the Cr^{3+} ion, i.e., the axial and twisted crystalline field of C_3 symmetry, are treated as perturbation on the trigonal states of the d^3 system of Cr^{3+}. By these treatments we attempt to describe the observed phenomena associated with the transitions between $^4A_{2g}$ and $^4T_{2g}$ states in Cr_2O_3. It is possible to reproduce the observed spectra of the polarization rotation and ellipticity, and the second-harmonic generation spectra described by the nonlinear susceptibilities χ^m and χ^e. The estimated theoretical magnitudes of these quantities are in reasonable agreement with the observed magnitudes. [S0163-1829(98)07415-3]

I. INTRODUCTION

In the 1960s, magneto-optical effects were studied for metals[1] and insulators.[2] In the 1990s, ellipsometry and broken time-reversal symmetry were extensively discussed theoretically[3,4] as well as experimentally[5] for the high-temperature superconductors. Reciprocity in reflection and transmission of light was studied by group-theoretical method.[6] Spontaneous nonreciprocal reflection of light[7] and its spectrum[8] were observed for Cr_2O_3. Here the interference between electric dipole and magnetic dipole is possible as the crystal loses space-inversion and time-reversal symmetry below the Néel temperature. First, Krichevtsov *et al.*[8] measured the spectra of the nonreciprocal rotation and ellipticity of light reflected from the antiferromagnetic Cr_2O_3 and found an ellipticity spectrum of dispersive type and a rotation spectrum of bell shape near 2.1 eV corresponding to the transition from $^4A_{2g}$ to $^4T_{2g}$ states. These look opposite to those expected from the Kramers-Kronig relation. This mystery will be solved in this paper. Second, Fiebig *et al.*[9] have succeeded in observing the antiferromagnetic domains in Cr_2O_3 through resonant second-harmonic signals due to the transitions between $^4A_{2g}$ and $^4T_{2g}$ states of a Cr^{3+} ion in the crystal. They also observed[10] the second-harmonic spectra described by the second-order magnetic and electric susceptibilities, χ^m and χ^e, separately and the interference effect between these contributions below Néel temperature $T_N = 307.5$ K. Muthukumar, Valenti, and Gros[11] proposed a microscopic theory to explain the observed nonreciprocal effect assuming a cluster model with D_{3d} symmetry. Unfortunately, their model does not reflect the correct symmetry of the cluster in the crystal which is $\bar{3}'$. Besides, in their treatment, only conventional trigonal crystalline fields with even and odd symmetry and spin-orbit interaction were assumed as perturbation on the trigonal states of the Cr^{3+} ion. We have shown, however, in a previous paper[12] that within this model both χ^m and χ^e vanish below T_N when the contributions from the four Cr^{3+} ions in a unit cell are summed up, even when each single-site contribution to χ^m or χ^e is finite. This is due to the fact that the real or imaginary nature of the matrix elements matters seriously in the problems of nonreciprocal optical effects in antiferromagnetic crystals, because we are forced to use complex wave functions in the ordered phase to evaluate them. In order to obtain nonvanishing nonlinear susceptibilities, twisted crystalline fields around the Cr^{3+} ion have to be introduced. The second purpose of the present paper is to evaluate the nonvanishing expressions of χ^m and χ^e so derived explicitly and to see if the calculated results are able to explain the observation, i.e., the magnitudes and the spectra of the susceptibilities and the interference effect.

In the present paper, we apply the same model both for the magnetoelectric spectrum of the nonreciprocal rotation and ellipticity of light and the second-harmonic generation (SHG) in antiferromagnetic Cr_2O_3.

In Sec. II we review the magnetic and electronic structures of the antiferromagnetic Cr_2O_3 crystal, and examine the types of the low-symmetry crystalline field involved, because these types are related to the reality of the relevant matrix elements contributing to the magnetoelectric effect and the second-harmonic generation. In Sec. III we derive expressions for the magnetoelectric susceptibilities for the spin-allowed transitions between the quartet states. The spin-forbidden transitions to the doublet states such as ^2E_g and $^2T_{1g}$ levels are also treated there. The results obtained in Sec. III are compared with the observed spectra of ellipticity and rotation in Sec. IV. We find that the observed features of the magnetoelectric spectra for the transition between $^4A_{2g}$ and $^4T_{2g}$ states are well explained. Estimation of the order of magnitude of these spectra is also made in good agreement with the observation. In contrast to this, we predict the conventional spectra of rotation and ellipticity for the transition from $^4A_{2g}$ to $^4T_{1g}$ states. The theory is also able to explain the observed spectra of spin-forbidden transitions. Contributions to the second-order susceptibilities χ^m and χ^e that are important in the resonance effect are derived explicitly in Sec. V. Their orders of magnitude are also estimated there. In Sec. VI, the second-harmonic spectra described by χ^m and χ^e are drawn using the results obtained in Sec. V. The agreement is satisfactory. However, it is found that the observed interference of χ^m and χ^e cannot be explained well because of the small phase difference between them. Two possible mechanisms are suggested to overcome this difficulty. Section VII is devoted to the conclusion. The Appendix gives some relevant reduced matrix elements of operators appearing in χ in terms of one-electron integrals together with the

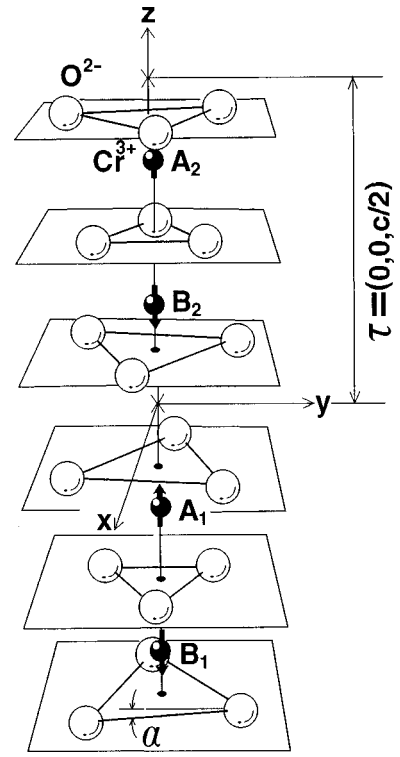

FIG. 1. The crystal and magnetic structure of Cr_2O_3 crystal below Néel temperature. Black and white circles represent Cr^{3+} and O^{2-} ions, respectively. The C_3 axis of the crystal is chosen as z axis, so the C_2 axis is chosen as x axis. The yz plane is the mirror plane. The origin of the coordinates is the inversion center. The arrows indicate the directions of the spins.

wave functions for the d^3 system (in the strong ligand-field limit).

II. MAGNETOLECTRIC AND NONLINEAR SUSCEPTIBILITIES

A. Magnetic and electronic structures of the crystal

Below Néel temperature $T_N = 307.5$ K, the crystal Cr_2O_3 loses the inversion and time-reversal symmetry and has the symmetry $R\bar{3}'c'$. The unit cell consists of four Cr ions, each surrounded by six oxygen ions as shown in Fig. 1. The z axis is taken along the threefold (C_3) axis of the crystal, and the x axis is taken along the twofold (C_2) axis of the crystal so that the yz plane is the mirror plane, in distinction from the choice of Refs. 8 and 11. We call the four ions located on the C_3 axis within the unit cell, from the lower to higher, B_1, A_1, B_2, and A_2 with down, up, down, and up spin in this order in one of the antiferromagnetic domains. In another domain, these spins are reversed simultaneously. We take the center of inversion between B_2 and A_1 as the origin. Then in the ordered phase described by the magnetic group, the ion A_1 with its environment is carried into B_1 by the operation $C_{2x}(\tau)$, into B_2 by ΘI and into A_2 by $\Theta\sigma_d(\tau)$, where τ is the displacement vector $(0,0,c/2)$ and Θ is the time-reversal operation. This implies that the wave functions of the four ions are related to each other by the following relations:

$$\Psi_i[B_1] = C_{2x}(\tau)\Psi_i[A_1], \tag{2.1}$$

$$\Psi_i[B_2] = \Theta I \Psi_i[A_1], \tag{2.2}$$

$$\Psi_i[A_2] = \Theta\sigma_d(\tau)\Psi_i[A_1]. \tag{2.3}$$

Take, for example, the ions at A_1 and B_1 [Eq. (2.1)]. We may adopt for the ith state (which may or may not necessarily be an eigenstate) of the ion B_1 the wave function obtained by transforming the ith state of the ion A_1, that is, rotating the latter by π around the x axis and translating it by τ. Note that Eqs. (2.1)–(2.3) are based on the symmetry of the magnetic group. They simply correlate the wave functions at different sites by the symmetry operations of the group. This procedure assumes that the molecular field acting on B_1 is obtained by just rotating by π the corresponding field on A_1. This is the symmetry described by the magnetic group. In this sense, the present treatment, which takes advantage of the magnetic symmetry throughout, is a mean field theory which neglects the spin fluctuations.

The matrix elements of an operator $\hat{A}$ at different sites are thus correlated to each other through the equations

$$\langle R\Psi|\hat{A}|R\Psi'\rangle = \langle\Psi|R^{-1}\hat{A}R|\Psi'\rangle, \tag{2.4}$$

$$\langle\Theta R\Psi|\hat{A}|\Theta R\Psi'\rangle = \langle\Psi|\Theta^{-1}R^{-1}\hat{A}R\Theta|\Psi'\rangle^*, \tag{2.5}$$

where R stands for any of the symmetry operations $C_{2x}(\tau)$, I, and $\sigma_d(\tau)$. Since both orbital and spin states are involved in the present problem, operator R as well as Θ act upon both of them. The matrix elements of x components of the magnetic- and electric-dipole moments, M_x and P_x, at B_1, A_2, and B_2 sites are related to those at A_1 by

$$M_x[B_1] = M_x[A_1], \quad P_x[B_1] = P_x[A_1], \tag{2.6}$$

$$M_x[A_2] = -M_x[A_1]^*, \quad P_x[A_2] = -P_x[A_1]^*, \tag{2.7}$$

$$M_x[B_2] = -M_x[A_1]^*, \quad P_x[B_2] = -P_x[A_1]^*. \tag{2.8}$$

These equations enable us to correlate the values of magnetoelectric and second-harmonic susceptibilities at B_1, B_2, and A_2 to that of A_1.

The optical absorption in Cr_2O_3 (Ref. 13) is similar to that of ruby[14] and is characterized by the two wide absorption bands due to transitions from the ground state $^4A_{2g}$ of the Cr^{3+} ion to the excited cubic-field terms $^4T_{2g}$ and $^4T_{1g}$. Below these bands, sharp lines are observed and assigned to the spin-forbidden transitions to ^2E_g and $^2T_{1g}$.[15] These are optical transitions between the multiplets with the same configuration $(t_2)^3$ as the ground state $^4A_{2g}$. On the other hand, the broad bands are due to the transitions to the states of the configuration $(t_2)^2e$ different from the ground states and their energies are nearly proportional to cubic crystalline field $10Dq$. Therefore these bands are broadened by strong electron-phonon interaction while the spin-forbidden levels ^2E_g and $^2T_{1g}$ do not suffer effectively from phonon broadenings so that they are much sharper. Taking account of these facts, we adopt the model of localized electrons on each Cr^{3+} ion in analyzing the magnetoelectric as well as the SHG spectrum.

Besides the cubic field, the Cr^{3+} ion is affected by the field of low symmetry V_{trig} corresponding to the symmetry

C_3 of the environment around the ion. The field $V_{\rm trig}$ can be written as a sum of the conventional trigonal field $V_{\rm axial}$ and the twisted field $V_{\rm twist}$ as

$$V_{\rm trig}=V_{\rm axial}+V_{\rm twist}, \tag{2.9}$$

$$V_{\rm axial}=V_{{\rm axial},g}+V_{{\rm axial},u}=V^c_{\rm trig}[T_{2g}x_0]+V_{\rm odd}[T_{1u}a_0], \tag{2.10}$$

$$V_{\rm twist}=V_{{\rm twist},g}+V_{{\rm twist},u}=V_{{\rm twist},g}[T_{1g}a_0]+V_{{\rm twist},u}[T_{2u}x_0]. \tag{2.11}$$

The $V_{{\rm axial},g}$ and $V_{{\rm axial},u}$ will be called conventional trigonal field in this paper, and denoted as $V^c_{\rm trig}\propto 3z^2-r^2$ and $V_{\rm odd}\propto z$, respectively. They have been assumed to be dominant in many previous treatments.[11,14] Note that they have C_{3v} symmetry around the z axis. From the real crystalline and spin structures of antiferromagnetic Cr_2O_3, however, we find that they also are affected by the twisted crystalline field $V_{\rm twist}=V_{{\rm twist},g}+V_{{\rm twist},u}$. The newly introduced crystalline field $V_{\rm twist}$ (Ref. 16) reflects the fact that the layers of three oxygen ions above and below a Cr^{3+} ion are twisted from each other. These crystalline fields are irreducible tensor operators with C_3 symmetry as denoted in Eqs. (2.10) and (2.11).[17] These fields $V_{\rm twist}$ have the following angular dependence: $V_{{\rm twist},g}\propto yz(3x^2-y^2)$ and $V_{{\rm twist},u}\propto y(3x^2-y^2)$.

It will be seen in the following sections that $V_{\rm axial}$ and $V_{\rm twist}$ contribute, respectively, to the magnetoelectric and the second-order susceptibilities.

The wave functions adapted to the O_h and C_3 symmetry for the ground and excited states will be called trigonal bases and are given in the Appendix for the three d electrons of a Cr^{3+} ion in a Cr_2O_3 crystal. They are used to evaluate the matrix elements of operators P_x and M_x.

The spin-orbit interaction $\mathcal{H}_{\rm so}$,

$$\mathcal{H}_{\rm so}=\sum_i \zeta \boldsymbol{s}_i\cdot\boldsymbol{l}_i, \tag{2.12}$$

may be put in the following form when working within the manifold of $({}^4A_{2g},{}^4T_{2g},{}^4T_{1g})$:[18]

$$\mathcal{H}_{\rm so}=\lambda \boldsymbol{S}\cdot\boldsymbol{L}, \tag{2.13}$$

where $\boldsymbol{S}$ and $\boldsymbol{L}$ are the total spin and the angular momentum operator, respectively. The parameter λ is equal to one-third of the single $3d$ electron spin-orbit coupling parameter ζ.

The effects of the spin-orbit interaction $\mathcal{H}_{\rm so}$ and the crystalline field of low symmetry $V_{\rm trig}$ will be taken into account as perturbation on these states. However, the first-order perturbation energies, i.e., diagonal components of these perturbations as well as the effects of the internal magnetic field, will be included in the unperturbed energies, e.g., for ${}^4A_{2g}$ and ${}^4T_{2g}$, as follows:

$$E({}^4A_{2g}M_s)=-\mu_B M_s H_i, \tag{2.14}$$

$$E({}^4T_{2g}M_s x_0)=E_0-\Delta E-\mu_B M_s H_i, \tag{2.15}$$

$$E({}^4T_{2g}M_s x_\pm)=E_0-\mu_B M_s H_i\pm\frac{1}{2}\lambda M_s, \tag{2.16}$$

where the nonmagnetic ground state is chosen as the origin of the energy, H_i is the internal magnetic field at the A_1 site, E_0 is the excitation energy to ${}^4T_{2g}x_m$, and ΔE is the splitting between ${}^4T_{2g}x_0$ and ${}^4T_{2g}x_m$ due to the crystalline field. The off-diagonal part of $V_{\rm trig}$ and $\mathcal{H}_{\rm so}$ put together is regarded as an essential perturbation and is denoted as $\mathcal{H}'$ in the following treatment.

B. Magnetoelectric susceptibility

The polarization rotation θ and ellipticity ϵ in the reflection on the crystal surface are described in terms of the magnetoelectric susceptibility $\alpha_\perp$ as[8,19]

$$\theta+i\epsilon=2\alpha_\perp\frac{1+n_\perp}{1-n_\perp}, \tag{2.17}$$

where $\alpha_\perp=\alpha_{xx}(\omega)=\alpha_{yy}(\omega)$ is the component of the magnetoelectric susceptibility tensor and $n_\perp$ is the refractive index given by $n_\perp^2=\varepsilon_{xx}(\omega)=\varepsilon_{yy}(\omega)$, i.e., the dielectric function in the xy plane. The contribution from Cr^{3+} ions at the A_1 site to the magnetoelectric susceptibility $\alpha_{xx}(\omega)$ is expressed as

$$\alpha_{xx,A_1}(\omega)=\frac{N}{\varepsilon_0 c\hbar}\sum_{i,n}\left\{\frac{\langle i|M_x|n\rangle\langle n|P_x|i\rangle}{\omega_{ni}-\omega-i\Gamma_{ni}}+\frac{\langle i|P_x|n\rangle\langle n|M_x|i\rangle}{\omega_{ni}+\omega+i\Gamma_{ni}}\right\}\rho_i, \tag{2.18}$$

where N is the number density of the unit cells, $\hbar\omega_{ni}=E_n-E_i$ is the excitation energy from the state i to n, Γ_{ni} is the dephasing rate, and ρ_i is the population distribution of the state i.

We write down expressions similar to Eq. (2.18) for other sites in the unit cell and sum up the contributions from the four sites. Then we find, by using the relations (2.6)–(2.8), that we may replace the numerators of Eq. (2.18) by $4{\rm Re}[\langle i|M_x|n\rangle\langle n|P_x|i\rangle]$ at the A_1 site simply to obtain the expression for the (total) magnetoelectric susceptibilty of the crystal. Note that $4N$ gives the number density of the Cr^{3+} ions. It will be needless to say that the result agrees with that derived previously by a different method.[19]

In Sec. III, only the resonance term of Eq. (2.18) will be dealt with, so that the expression to be used hereafter reads

$$\alpha_{xx}(\omega)=\frac{4N}{\varepsilon_0 c\hbar}\sum_{i,n}\frac{{\rm Re}[M_{in}P_{ni}]}{\omega_{ni}-\omega-i\Gamma_{ni}}\rho_i. \tag{2.19}$$

The thermal distribution ρ_i depends on the spin polarization of the ground state ${}^4A_{2g}$ at the site A_1. The bases $|i\rangle$ and $|n\rangle$ in evaluating the matrices $M_{in}\equiv\langle i|M_x|n\rangle$ and $P_{ni}\equiv\langle n|P_x|i\rangle$ in Eq. (2.19) should be the eigenfunctions which diagonalize the spin-orbit interaction $\mathcal{H}_{\rm so}$ and the crystalline field. Since we start from the cubic-field terms and include the diagonal elements of $\mathcal{H}_{\rm so}$ and $V_{\rm trig}$ in the unperturbed energy of the cubic-field terms as mentioned above, only the off-diagonal components of $\mathcal{H}_{\rm so}$ and $V_{\rm trig}$ appear in the perturbed expressions of the numerators in Eq. (2.19).

C. Second-order susceptibilities

Second-order optical susceptibility $\chi(2\omega;\omega,\omega)$ under nearly resonant pumping of the ${}^4T_{2g}$ state of the Cr^{3+} ion comes from two processes. In one process, two fundamental

photons excite the ion virtually from the ground $^4A_{2g}$ state to the $^4T_{2g}$ state through the two successive electric-dipole transitions and then the second harmonics are generated by the magnetic-dipole transition back to the ground state. This is described by the susceptibility $\chi^m \equiv \chi^{mee}_{xxx}(2\omega,\omega,\omega)$. In another process, the excitation process is the same as the former case and the second harmonics are generated by the electric-dipole transition. This is described by $\chi^e \equiv \chi^{eee}_{xxx}(2\omega,\omega,\omega)$. The superscripts $m(e)$ and two e's of χ indicate the magnetic (electric) dipole moment $M_x(P_x)$ for the second harmonics and the two electric-dipole moments P_x and P_x for the two fundamentals in this order, and subscripts x, x, and x denote the polarization directions of the dipole moments in the same order, where z and x axes have been chosen along the threefold (C_3) and twofold (C_{2x}) axes of the Cr_2O_3 crystal, respectively. Note that the present choice is different from that of Fiebig *et al.*[10]

First, let us write down the expressions for χ^m and χ^e under off-resonant conditions where the damping effect is negligible. These χ's are the contribution from the Cr^{3+} ions at the A_1 site (see below). With N the number density of unit cells and n the refractive index for the fundamentals, respectively, the expression for χ^m is given by

$$\chi^m=\frac{Nn}{\epsilon_0 c\hbar^2}\sum_i\left(\sum_{m,k}\frac{(MPP)_{imki}}{(\omega_{mi}-2\omega)(\omega_{ki}-\omega)}+\sum_{m,m'}\frac{(PMP)_{imm'i}}{(\omega_{mi}+\omega)(\omega_{m'i}-\omega)}+\sum_{k,m}\frac{(PPM)_{ikmi}}{(\omega_{mi}+2\omega)(\omega_{ki}+\omega)}\right)\rho_i, \tag{2.20}$$

where ω_{mi}, for example, is the energy difference between the states $|m\rangle$ and $|i\rangle$ (divided by $\hbar$) and

$$(MPP)_{imki}=(M_x)_{im}(P_x)_{mk}(P_x)_{ki}, \tag{2.21}$$

$$(PMP)_{imm'i}=(P_x)_{im}(M_x)_{mm'}(P_x)_{m'i}, \tag{2.22}$$

$$(PPM)_{ikmi}=(P_x)_{ik}(P_x)_{km}(M_x)_{mi}, \tag{2.23}$$

and $\rho_i=\rho(^4A_{2g}M_s)$ describes thermal distribution in the ground state $^4A_{2g}$.

The electric-dipole contribution to the second-harmonic generation χ^e is calculated in a similar way:

$$\chi^e=\frac{N}{\epsilon_0\hbar^2}\sum_i\left(\sum_{m,k}\frac{(\bar{P}PP)_{imki}}{(\omega_{mi}-2\omega)(\omega_{ki}-\omega)}+\sum_{m,m'}\frac{(P\bar{P}P)_{imm'i}}{(\omega_{mi}+\omega)(\omega_{m'i}-\omega)}+\sum_{k,m}\frac{(PP\bar{P})_{ikmi}}{(\omega_{mi}+2\omega)(\omega_{ki}+\omega)}\right)\rho_i, \tag{2.24}$$

where

$$(\bar{P}PP)_{imki}=(P_x)_{im}(P_x)_{mk}(P_x)_{ki}, \tag{2.25}$$

$$(P\bar{P}P)_{imm'i}=(P_x)_{im}(P_x)_{mm'}(P_x)_{m'i}, \tag{2.26}$$

$$(PP\bar{P})_{ikmi}=(P_x)_{ik}(P_x)_{km}(P_x)_{mi}. \tag{2.27}$$

We have considered here the case where both the fundamental and second harmonics are linearly polarized along the C_{2x} axis. Other components of the tensor χ are derived by the symmetry consideration as shown in Sec. VI.

On summing up the contributions from the four Cr^{3+} ions in the unit cell by using relations (2.6)–(2.8), we have χ^m_{total} below T_N as

$$\chi^m_{\text{total}}=\frac{4Nn}{\epsilon_0 c\hbar^2}\sum_i\left(\sum_{m,k}\frac{i\ \text{Im}(MPP)_{imki}}{(\omega_{mi}-2\omega)(\omega_{ki}-\omega)}+\sum_{m,m'}\frac{i\ \text{Im}(PMP)_{imm'i}}{(\omega_{mi}+\omega)(\omega_{m'i}-\omega)}+\sum_{m,k}\frac{i\ \text{Im}(PPM)_{ikmi}}{(\omega_{mi}+2\omega)(\omega_{ki}+\omega)}\right)\rho_i, \tag{2.28}$$

$$\chi^e_{\text{total}}=\frac{4N}{\epsilon_0\hbar^2}\sum_i\left(\sum_{m,k}\frac{i\ \text{Im}(\bar{P}PP)_{imki}}{(\omega_{mi}-2\omega)(\omega_{ki}-\omega)}+\sum_{m,m'}\frac{i\ \text{Im}(P\bar{P}P)_{imm'i}}{(\omega_{mi}+\omega)(\omega_{m'i}-\omega)}+\sum_{k,m}\frac{i\ \text{Im}(PP\bar{P})_{ikmi}}{(\omega_{mi}+2\omega)(\omega_{ki}+\omega)}\right)\rho_i\ . \tag{2.29}$$

In the subsequent treatments, we are mainly interested in the resonance effect, so that only the first term of these expressions will be kept hereafter, and the subscript ''total'' will be dropped for simplicity when there is no fear of confusion:

$$\chi^m=\frac{4Nn}{\epsilon_0 c\hbar^2}\sum_{i,m,k}\rho_i\frac{i\ \text{Im}(MPP)_{imki}}{(\omega_{mi}-2\omega)(\omega_{ki}-\omega)}, \tag{2.30}$$

$$\chi^e=\frac{4N}{\epsilon_0\hbar^2}\sum_{i,m,k}\rho_i\frac{i\ \text{Im}(\bar{P}PP)_{imki}}{(\omega_{mi}-2\omega)(\omega_{ki}-\omega)}. \tag{2.31}$$

Probably, it is worth pointing out that these expressions remain valid also in the paramagnetic phase, where the space group is $R\bar{3}c$ and the time-reversal operation Θ is no longer involved. This can be seen as follows. First of all, we write

$$2i\ \text{Im}(MPP)=(MPP)-(MPP)^*, \tag{2.32}$$

$$2i\ \text{Im}(\bar{P}PP)=(\bar{P}PP)-(\bar{P}PP)^*. \tag{2.33}$$

Next, we remember that

$$\langle\Phi|\Theta^{-1}\hat{A}\Theta|\Psi\rangle^*=\langle\Theta\Phi|\hat{A}|\Theta\Psi\rangle. \tag{2.34}$$

If the suffix $i^\dagger$ is defined by

$$\Theta\Phi_i=\Phi_{i^\dagger}, \tag{2.35}$$

then, we have, for example,

$$(M_x)_{im}{}^* = -(M_x)_{i^\dagger m^\dagger}, \quad (P_x)_{im}{}^* = (P_x)_{i^\dagger m^\dagger}. \quad (2.36)$$

These relations enable us to replace the second term on the right-hand side of Eqs. (2.32) and (2.33) by the first term but with daggered suffixes, that is,

$$-(MPP)^*_{imki} = (MPP)_{i^\dagger m^\dagger k^\dagger i^\dagger},$$

$$-(\overline{P}PP)^*_{imki} = -(\overline{P}PP)_{i^\dagger m^\dagger k^\dagger i^\dagger}. \quad (2.37)$$

Since Φ_i has the same energy as $\Phi_{i^\dagger}$ in the paramagnetic phase, it is not difficult to arrive at the expressions

$$\chi^m = \frac{4Nn}{\epsilon_0 c\hbar^2}\sum_{i,m,k}\rho_i \frac{(MPP)_{imki}}{(\omega_{mi}-2\omega)(\omega_{ki}-\omega)}, \quad (2.38)$$

$$\chi^e = 0, \quad (2.39)$$

which are valid in this phase. These equations also follow from Eqs. (2.20) and (2.24) by making use of the equations

$$M_x[B_1] = M_x[A_1], \quad P_x[B_1] = P_x[A_1], \quad (2.40)$$

$$M_x[A_2] = M_x[A_1], \quad P_x[A_2] = -P_x[A_1], \quad (2.41)$$

$$M_x[B_2] = M_x[A_1], \quad P_x[B_2] = -P_x[A_1], \quad (2.42)$$

which follow from the relations

$$\Psi_i[B_1] = C_{2x}(\boldsymbol{\tau})\Psi_i[A_1], \quad (2.43)$$

$$\Psi_i[B_2] = I\Psi_i[A_1], \quad (2.44)$$

$$\Psi_i[A_2] = \sigma_d(\boldsymbol{\tau})\Psi_i[A_1], \quad (2.45)$$

valid in the paramagnetic phase.

III. MAGNETOELECTRIC SPECTRA

We are interested in the magnetoelectric spectrum under nearly resonant pumping from the ground state $^4A_{2g}$ into (1) the spin-allowed bands $^4T_{2g}$ and $^4T_{1g}$ and (2) the spin-forbidden levels ^2E_g and $^2T_{1g}$. The former processes are analyzed in Sec. III A and the latter in Sec. III B.

A. Spin-allowed transitions

In order to evaluate the magnetoelectric susceptibility of Eq. (2.19), we need the following matrix elements for the transition from the ground state $^4A_{2g}M_s$ to the band $^4T_{2g}M_sx_m$ at the A_1 site:[17]

$$\langle {}^4A_{2g}M_s|M_x|{}^4T_{2g}M_s x_{\mp}\rangle$$

$$= -\frac{\mu_B}{2}\sum_{\pm}\langle {}^4A_{2g}M_s|L_{\pm}|{}^4T_{2g}M_s x_{\mp}\rangle$$

$$= \mp 2\sqrt{2}i\left(\frac{\mu_B}{2}\right), \quad (3.1)$$

$$\langle {}^4T_{2g}M_s x_{\mp}|\overline{P_x}|{}^4A_{2g}M_s\rangle = \frac{i}{2\sqrt{3}}\langle {}^4T_{2g}\|\overline{P_x}[T_1]\|{}^4A_{2g}\rangle. \quad (3.2)$$

Here the electric-dipole moment P_x is accompanied with the crystalline field $V_{\text{axial},u} \equiv V[T_{1u}a_0]$, i.e., the conventional crystalline field V_{odd} of odd parity, which has been used for analysis of the ruby spectrum. The effect of this crystalline field is taken into account as perturbation on both states linked by the electric-dipole moment. The combined effect of the electric-dipole moment $P_x = P_x[T_{1u}a_\pm]$ and the crystalline field $V_{\text{odd}} = V[T_{1u}a_0]$ leads to the effective dipole moment denoted as $\overline{P_x}$ and defined by

$$\langle i|\overline{P_x}|n\rangle = -\sum_{j'}\frac{\langle i|P_x|j'\rangle\langle j'|V_{\text{odd}}|n\rangle}{\Delta E(j'n)} - \sum_{j'}\frac{\langle i|V_{\text{odd}}|j'\rangle\langle j'|P_x|n\rangle}{\Delta E(j'i)}, \quad (3.3)$$

with $\Delta E(j'n) = E(j') - E(n)$. The j'-dependent energy denominators $\Delta E(j'n)$, etc. may be approximated by an average excitation energy to odd states ΔE_o. Then the enclosure relation enables us to decompose $\overline{P_x}$ into its irreducible components as

$$\overline{P_x} = -\frac{1}{2\sqrt{3}}\sum_{m=\pm} m\overline{P_x}[T_2x_m] + \frac{1}{\sqrt{6}}\sum_{m=\pm} m\overline{P_x}[Eu_m] + \frac{i}{2}\sum_{m=\pm}\overline{P_x}[T_1a_m], \quad (3.4)$$

by the help of the Clebsch-Gordan coefficients. The relevant matrix elements are evaluated also by means of the Wigner-Eckart theorem and the many-electron wave functions in the Appendix as

$$\langle {}^4T_{2g}x_{\mp}|\overline{P_x}|{}^4A_{2g}\rangle = \frac{i}{2\sqrt{3}}\langle {}^4T_{2g}\|\overline{P_x}[T_1]\|{}^4A_{2g}\rangle = \frac{i}{\sqrt{2}}(-\langle u_{\pm}|\overline{p_x}|x_{\mp}\rangle \mp \langle u_{\mp}|\overline{p_x}|x_0\rangle). \quad (3.5)$$

Thus the product of Eqs. (3.1) and (3.5) is real so that this channel can contribute to α_{xx}. Other components of the crystalline field in Eq. (2.11) have no contribution to the present magnetoelectric susceptibility α_{xx}.

As to the resonant excitation to the state $|{}^4T_{1g}a_\pm\rangle$, we need the following matrix elements:

$$\langle {}^4T_{1g}a_{\pm}|\overline{P_x}|{}^4A_{2g}\rangle = \pm\frac{1}{6}\langle {}^4T_{1g}\|\overline{P_x}[T_2]\|{}^4A_{2g}\rangle = \frac{-1}{\sqrt{2}}(\pm\langle u_{\mp}|\overline{p_x}|x_{\pm}\rangle + \langle u_{\pm}|\overline{p_x}|x_0\rangle). \quad (3.6)$$

Here also the Wigner-Eckart theorem and the many-electron wave functions in the Appendix were used. The one-electron orbitals can be expressed in terms of real orbitals so that it is easy to confirm $\langle {}^4T_{2g}x_{\pm}|\overline{P_x}|{}^4A_{2g}\rangle$ in Eq. (3.5) to be pure imaginary while $\langle {}^4T_{1g}a_{\pm}|\overline{P_x}|{}^4A_{2g}\rangle$ in Eq. (3.6) is real. The matrix element $\langle {}^4A_{2g}|M_x|{}^4T_{1g}a_{\pm}\rangle$ vanishes. Therefore we need to take into account the perturbation of spin-orbit inter-

action working on $|^4T_{1g}a_\pm\rangle$ which makes the magnetic-dipole transition possible to the state $|^4T_{1g}a_\pm\rangle$ as follows:

$$\begin{aligned}&\langle {}^4A_{2g}M_s|\overline{M_x}|{}^4T_{1g}M_s a_\pm\rangle\\&=\left(-\frac{\mu_B}{2}\right)\sum_m \langle {}^4A_{2g}M_s|L_{-m}|{}^4T_{2g}M_s x_m\rangle\\&\quad\times\frac{\langle {}^4T_{2g}M_s x_m|\mathcal{H}_{\rm so}|{}^4T_{1g}M_s a_\pm\rangle}{E({}^4T_{1g}M_s a_\pm)-E({}^4T_{2g}M_s x_m)}\\&=\left(\frac{\mu_B}{2}\right)(\mp 2\sqrt{2}i)\frac{i\lambda M_s}{2\Delta E_1}=\pm\frac{\mu_B\lambda M_s}{\sqrt{2}\Delta E_1},\end{aligned}\tag{3.7}$$

where

$$\Delta E_1\equiv E({}^4T_{2g}M_s x_\pm)-E({}^4T_{1g}M_s a_\pm).\tag{3.8}$$

The matrix elements of spin-orbit interaction $\mathcal{H}_{\rm so}$ are evaluated by using the Wigner-Eckart theorem and Table II of Ref. 20 as

$$\begin{aligned}&\langle {}^4T_{2g}M_s x_\pm|\mathcal{H}_{\rm so}|{}^4T_{1g}M_s a_\pm\rangle\\&=\langle {}^4T_{2g}\|V_{\rm so}\|{}^4T_{1g}\rangle\frac{1}{2\sqrt{3}}\left\langle\frac{3}{2}M_s\middle|\frac{3}{2}M_s 10\right\rangle\\&\quad\times\langle T_2 x_\pm|T_1 a_\pm T_1 a_0\rangle\\&=\frac{i}{2}M_s\lambda,\end{aligned}\tag{3.9}$$

with $\lambda\equiv\zeta/3$. The double barred matrix element $\langle t_2\|v_{\rm so}\|t_2\rangle$ of the spin-orbit interaction for a t_2 electron is given by $3i\zeta$.

Now we can evaluate the magnetoelectric susceptibility $\alpha_{xx}(\omega)$ for the spin-allowed transitions. Under nearly resonant pumping of $^4T_{2g}x_\pm$, $\alpha_{xx}(\omega)$ is obtained by inserting Eqs. (3.1) and (3.2) into Eq. (2.19) as follows:

$$\begin{aligned}\alpha_{xx}^{(a)}(\omega)&=\alpha_{yy}^{(a)}(\omega)\\&=-A_0\sum_{M_s}\rho(M_s)\\&\quad\times\left\{\frac{1}{E({}^4T_{2g}M_s x_+)-E({}^4A_{2g}M_s)-\omega-i\Gamma_a}\right.\\&\quad\left.-\frac{1}{E({}^4T_{2g}M_s x_-)-E({}^4A_{2g}M_s)-\omega-i\Gamma_a}\right\}\\&\simeq A\frac{\{(E^*-\omega)^2-\Gamma_a^2\}+2i\Gamma_a(E^*-\omega)}{(E^*-\omega)^2+\Gamma_a^2},\end{aligned}\tag{3.10}$$

where

$$E^*=\sum_\pm\frac{1}{2}\{E({}^4T_{2g}M_s x_\pm)-E({}^4A_{2g}M_s)\},$$

$$A_0=\frac{N}{\sqrt{6}}\frac{\mu_B}{\epsilon_0 c}\langle {}^4T_{2g}\|\overline{P_x}[T_1]\|{}^4A_{2g}\rangle,\quad\text{and}\quad A=A_0\lambda\langle M_s\rangle.\tag{3.11}$$

Here we include the diagonal components of $\mathcal{H}_{\rm so}$ in the eigenenergies, i.e.,

$$E({}^4T_{2g}M_s x_\pm)=E_0\pm\frac{1}{2}\lambda M_s,\quad\text{and}\quad\langle M_s\rangle\equiv\sum_{M_s}M_s\rho(M_s),\tag{3.12}$$

and neglect M_s dependence of the energy denominator in Eq. (3.10) where $\langle M_s\rangle$ denotes the magnetization at sublattice A_1. Here and hereafter (Secs. III and IV) we set $\hbar=1$ for simplicity. The spin-orbit interaction in Eq. (3.12) is evaluated in a way similar to Eq. (3.9) as follows:

$$\begin{aligned}&\langle {}^4T_{2g}M_s x_\pm|\mathcal{H}_{\rm so}|{}^4T_{2g}M_s x_\pm\rangle\\&=\langle {}^4T_{2g}\|V_{\rm so}\|{}^4T_{2g}\rangle\frac{1}{2\sqrt{3}}\left\langle\frac{3}{2}M_s\middle|\frac{3}{2}M_s 10\right\rangle\\&\quad\times\langle T_2 x_\pm|T_2 x_\pm T_1 a_0\rangle\\&=-\frac{\sqrt{5}}{3\sqrt{2}}(3i\zeta)\frac{M_s}{3\sqrt{3}}\sqrt{\frac{3}{5}}\left(\frac{\pm i}{\sqrt{2}}\right)\\&=\pm\frac{M_s}{2}\lambda.\end{aligned}\tag{3.13}$$

The magnetoelectric spectrum $\alpha_{xx}^{(b)}(\omega)$ at $^4T_{1g}a_m$ is theoretically derived to show characteristics different from that of $^4T_{2g}x_\pm$. Both the matrix elements of $\overline{P_x}$ [Eq. (3.6)] and $\overline{M_x}$ [Eq. (3.7)] are real, resulting in the finite contribution even after summing over four ions in the unit cell. The magnetoelectric susceptibility $\alpha_{xx}^{(b)}(\omega)$ is expressed as

$$\begin{aligned}\alpha_{xx}^{(b)}(\omega)&=\alpha_{yy}^{(b)}(\omega)\\&=-\sum_{M_s}\sum_\pm\frac{B(M_s)\rho(M_s)}{E({}^4T_{1g}M_s a_\pm)-E({}^4A_{2g}M_s)-\omega-i\Gamma_b},\end{aligned}\tag{3.14}$$

where $B(M_s)=-A_0\lambda M_s/\Delta E_1$. First, when we neglect M_s dependence of energy denominator, $\alpha_{xx}^{(b)}(\omega)$ is proportional to the sublattice magnetization $\langle M_s\rangle$. Therefore both $\alpha_{xx}^{(a)}$ and $\alpha_{xx}^{(b)}$ are finite only below Néel temperature in accordance with the fact that the system loses both inversion and time-reversal symmetry below Néel temperature. Second, we have included the relaxation rates Γ_a and Γ_b in Eqs. (3.10) and (3.14) in accordance with causality requirement. The real and imaginary parts of $-2\alpha_{xx}(\omega)(n_\perp+1)/(n_\perp-1)$ describe the polarization rotation and ellipticity of light reflected at the crystal surface, respectively. Usually, as Eq. (3.14) shows, the rotation spectrum $\theta(\omega)$ is dispersive while the ellipticity spectrum is of absorptive type. This is the case of $^4T_{1g}a_\pm$. The spectrum characteristics are reversed for the case of $^4T_{2g}x_\pm$ as Eq. (3.10) shows. This comes from the fact that two levels $^4T_{2g}M_s x_+$ and $^4T_{2g}M_s x_-$ are split off by the spin-orbit interaction $\lambda M_s(<\Gamma_a)$, and contribute to the magnetoelectric spectrum with opposite sign. These features of the spectrum appear to be in agreement with the observed spectra,[8] as will be shown in the next section. On the other hand, two states of $^4T_{1g}M_s a_\pm$ have the contribution with the same sign so that the magnetoelectric susceptibility is of ordinary type.

B. Spin-forbidden transition

In this subsection, we will propose a microscopic model to explain the magnetoelectric spectra of the spin-forbidden transitions to ^2E_g and $^2T_{1g}$ from the ground state $^4A_{2g}$.

The magnetic-dipole transition between the level ^2E_g and the ground state $^4A_{2g}$ becomes possible with assistance of the spin-orbit interaction $\mathcal{H}_{\rm so}$. This matrix element is evaluated by perturbational method as

$$\begin{aligned}\langle {}^4A_{2g}M_s|\overline{M}_x|{}^2E_gM_s'u_m\rangle &= \left(-\frac{\mu_B}{2}\right)\sum_{\pm}\langle {}^4A_{2g}M_s|L_{\mp}|{}^4T_{2g}M_sx_{\pm}\rangle \\ &\times\frac{\langle {}^4T_{2g}M_sx_{\pm}|\mathcal{H}_{\rm so}|{}^2E_gM_s'u_m\rangle}{E({}^2E_gM_s'u_m)-E({}^4T_{2g}M_sx_{\pm})}. \qquad (3.15)\end{aligned}$$

As long as we discuss the case of such low temperatures as $T\ll T_N$, we may choose the ground state $^4A_{2g}M_s=3/2$ at the A_1 sublattice and then we have the finite matrix element of Eq. (3.15) only for the level $|{}^2E_gM_s'=1/2u_-\rangle$. The matrix element of spin-orbit interaction in Eq. (3.15) is calculated by using the Wigner-Eckart theorem and the Wigner and the Clebsch-Gordan coefficients as follows:[20]

$$\begin{aligned}&\langle {}^4T_{2g}3/2x_+|\mathcal{H}_{\rm so}|{}^2E_g1/2u_-\rangle \\ &=\langle {}^4T_{2g}\|V_{\rm so}\|{}^2E_g\rangle(-1)\frac{1}{2}\left\langle\frac{3}{2}\,\frac{3}{2}1-1\middle|\frac{1}{2}\,\frac{1}{2}\right\rangle \\ &\quad\times\langle T_2x_+T_1a_+|Eu_-\rangle \\ &=\frac{2\sqrt{2}}{3}(3\sqrt{2}i\zeta)\left(\frac{-1}{2}\right)\frac{1}{\sqrt{2}}\left(-\frac{i}{\sqrt{3}}\right) \\ &=-\sqrt{\frac{2}{3}}\zeta. \qquad (3.16)\end{aligned}$$

Then Eq. (3.15) is obtained as

$$\begin{aligned}&\langle {}^4A_{2g}3/2|\overline{M}_x|{}^2E_g1/2u_-\rangle \\ &=\left(-\frac{\mu_B}{2}\right)(-2\sqrt{2}i)\left(-\sqrt{\frac{2}{3}}\zeta\right)/\Delta E_{dq} \\ &=\sqrt{2}i\mu_B\left(-\sqrt{\frac{2}{3}}\zeta/\Delta E_{dq}\right), \qquad (3.17)\end{aligned}$$

where $\Delta E_{dq}\equiv E({}^2E_g1/2u_-)-E({}^4T_{2g}3/2x_+)$. The effective electric-dipole moment $\overline{\overline{P}}_x$ is also evaluated in a similar way as

$$\begin{aligned}\langle {}^2E_g1/2u_-|\overline{\overline{P}}_x|{}^4A_{2g}3/2\rangle &= \frac{\langle {}^2E_g1/2u_-|\mathcal{H}_{\rm so}|{}^4T_{2g}3/2x_+\rangle}{E({}^2E_g1/2u_-)-E({}^4T_{2g}3/2x_+)} \\ &\times\langle {}^4T_{2g}3/2x_+|\overline{P}_x|{}^4A_{2g}3/2\rangle \\ &=\left(-\sqrt{\frac{2}{3}}\zeta/\Delta E_{dq}\right)\left(\frac{i}{2\sqrt{3}}\right) \\ &\times\langle {}^4T_{2g}\|\overline{P}_x[T_1]\|{}^4A_{2g}\rangle. \qquad (3.18)\end{aligned}$$

Therefore the magnetoelectric susceptibility at $^2E_g1/2u_-$ is finally expressed as

$$\alpha_{xx}^{(c)}(\omega)=-\frac{A_0(\sqrt{2/3}\zeta/\Delta E_{dq})^2}{E({}^2E_g1/2u_-)-E({}^4A_{2g}3/2)-\omega-i\Gamma_c}. \qquad (3.19)$$

Note that the ellipticity spectrum $\epsilon(\omega)=-2\mathrm{Im}[\alpha_{xx}^{(c)}(\omega)](n_\perp+1)/(n_\perp-1)$ is of Lorentzian form, i.e., of absorptive type, and that the rotation spectrum $\theta(\omega)=-2\mathrm{Re}[\alpha_{xx}^{(c)}(\omega)](n_\perp+1)/(n_\perp-1)$ is of dispersive type in contrast to those at $^4T_{2g}$.

The spin-orbit interaction is smaller than but of the same order of magnitude as the internal magnetic field splitting. Therefore it is a better approximation to diagonalize the spin-orbit interaction $\mathcal{H}_{\rm so}$ within the manifold of $^4T_{2g}M_sx_m$. The state $|{}^4T_{2g}3/2x_-\rangle$ is coupled to $|{}^4T_{2g}1/2x_0\rangle$ and $|{}^4T_{2g}-1/2x_+\rangle$ by the matrix

$$\begin{bmatrix} -\frac{3}{2}\mu_BH_i+\frac{1}{2}K-\frac{3}{4}\lambda & \frac{1}{2}\sqrt{\frac{3}{2}}\lambda & 0 \\ \frac{1}{2}\sqrt{\frac{3}{2}}\lambda & -\frac{1}{2}\mu_BH_i-K & \sqrt{\frac{1}{2}}\lambda \\ 0 & \sqrt{\frac{1}{2}}\lambda & \frac{1}{2}\mu_BH_i+\frac{1}{2}K-\frac{1}{4}\lambda \end{bmatrix}, \qquad (3.20)$$

where H_i denotes the internal field and $K=\langle x_m|v_{\rm trig}^c|x_m\rangle=-(\sqrt{2}/3)\langle {}^4T_{2g}\|V[T_{2g}x_0]\|{}^4T_{2g}\rangle$ is the strength of the conventional trigonal field, so that ΔE in Eq. (2.15) is given by $\frac{3}{2}K$. When the lowest eigenstate $|{}^4T_{2g}3/2x_-^*\rangle$ is denoted by

$$|{}^4T_{2g}3/2x_-^*\rangle=\alpha|3/2x_-\rangle+\beta|1/2x_0\rangle+\gamma|-1/2x_+\rangle, \qquad (3.21)$$

the state $|{}^2E_g-1/2u_+\rangle$ is shown to contribute to the magnetoelectric susceptibility with the same order of perturbations as from $|{}^2E_g1/2u_-\rangle$. The effective magnetic-dipole moment $\overline{M}_x$ and electric one $\overline{\overline{P}}_x$ are evaluated in terms of the coefficients α, β, and γ as follows:

$$\begin{aligned}&\langle {}^4A_{2g}3/2|\overline{M}_x|{}^2E_g-1/2u_+\rangle \\ &=\langle {}^4A_{2g}3/2|M_x|{}^4T_{2g}3/2x_-^*\rangle \\ &\quad\times\frac{\langle {}^4T_{2g}3/2x_-^*|\mathcal{H}_{\rm so}|{}^2E_g-1/2u_+\rangle}{E({}^2E_g-1/2u_+)-E({}^4T_{2g}3/2x_-^*)} \\ &=\alpha(-\sqrt{2}i\mu_B)\{\beta^*\langle {}^4T_{2g}1/2x_0|\mathcal{H}_{\rm so}|{}^2E_g-1/2u_+\rangle \\ &\quad+\gamma^*\langle {}^4T_{2g}-1/2x_+|\mathcal{H}_{\rm so}|{}^2E_g-1/2u_+\rangle\}/\Delta E_{dq} \\ &=(-\sqrt{2}i\mu_B)\left(\sqrt{\frac{2}{3}}\zeta/\Delta E_{dq}\right) \\ &\quad\times\alpha(\beta^*/\sqrt{3}-2\gamma^*/\sqrt{15}), \qquad (3.22)\end{aligned}$$

where the energy denominator $E({}^2E_g-1/2u_+)-E({}^4T_{2g}3/2x_-^*)$ is approximated to be equal to ΔE_{dq}, and

$$\langle {}^2E_g-1/2u_+|\overline{\overline{P}}_x|{}^4A_{2g}3/2\rangle$$
$$=\frac{\langle {}^2E_g-1/2u_+|\mathcal{H}_{\rm so}|{}^4T_{2g}3/2x_-^*\rangle}{E({}^2E_g-1/2u_+)-E({}^4T_{2g}3/2x_-^*)}$$
$$\times\langle {}^4T_{2g}3/2x_-^*|\overline{P}_x|{}^4A_{2g}3/2\rangle$$
$$=\frac{i}{2\sqrt{3}}\langle {}^4T_{2g}\|\overline{P}_x[T_1]\|{}^4A_{2g}\rangle\left(\sqrt{\frac{2}{3}}\zeta/\Delta E_{dq}\right)$$
$$\times\alpha^*(\beta/\sqrt{3}-2\gamma/\sqrt{15}). \quad (3.23)$$

As a result, the magnetoelectric susceptibility at $|{}^2E_g-1/2u_+\rangle$ is evaluated as follows:

$$\alpha_{xx}^{(c')}(\omega)=\frac{A_0(\sqrt{2/3}\zeta/\Delta E_{dq})^2R}{E({}^2E_g-1/2u_+)-E({}^4A_{2g}3/2)-\omega-i\Gamma_{c'}}, \quad (3.24)$$

with

$$R=\left|\frac{\alpha}{\sqrt{3}}\left(\beta^*-\frac{2}{\sqrt{5}}\gamma^*\right)\right|^2. \quad (3.25)$$

It is noted here that the signal Eq. (3.24) at $|{}^2E_g-1/2u_+\rangle$ has the opposite sign from that, Eq. (3.19), at $|{}^2E_g1/2u_-\rangle$.

Finally we will discuss the magnetoelectric spectrum at ${}^2T_{1g}$. For this purpose, we need the following matrix elements of spin-orbit interaction:

$$\langle {}^2T_{1g}1/2a_-|\mathcal{H}_{\rm so}|{}^4T_{2g}3/2x_+\rangle$$
$$=-\langle {}^2T_{1g}\|V_{\rm so}\|{}^4T_{2g}\rangle\frac{1}{\sqrt{2}}\frac{1}{\sqrt{3}}\left\langle\frac{1}{2}\frac{1}{2}\middle|\frac{3}{2}\frac{3}{2}1-1\right\rangle$$
$$\times\langle T_1a_-|T_2x_+T_1a_+\rangle$$
$$=-(\sqrt{6}i\zeta)\frac{1}{\sqrt{6}}\frac{1}{\sqrt{2}}\sqrt{\frac{2}{3}}$$
$$=-\frac{i}{\sqrt{3}}\zeta, \quad (3.26)$$

$$\langle {}^2T_{1g}1/2a_0|\mathcal{H}_{\rm so}|{}^4T_{2g}3/2x_-\rangle$$
$$=-\langle {}^2T_{1g}\|V_{\rm so}\|{}^4T_{2g}\rangle\frac{1}{\sqrt{2}}\frac{1}{\sqrt{3}}\left\langle\frac{1}{2}\frac{1}{2}\middle|\frac{3}{2}\frac{3}{2}1-1\right\rangle$$
$$\times\langle T_1a_0|T_2x_-T_1a_+\rangle$$
$$=-(\sqrt{6}i\zeta)\frac{1}{\sqrt{6}}\frac{1}{\sqrt{2}}\frac{1}{\sqrt{6}}$$
$$=-\frac{i}{2\sqrt{3}}\zeta. \quad (3.27)$$

The effective magnetic- and electric-dipole moments are obtained by using Eqs. (3.26) and (3.27) similarly to Eqs. (3.17) and (3.18). The effective magnetic- and electric-dipole moments coupled by the spin-orbit interaction through the state ${}^4T_{2g}$ are both real:

$$\langle {}^4A_{2g}3/2|\overline{M}_x|{}^2T_{1g}1/2a_0\rangle=\frac{1}{\sqrt{6}}\frac{\mu_B\zeta}{\Delta E'_{dq}},$$
$$\langle {}^4A_{2g}3/2|\overline{M}_x|{}^2T_{1g}1/2a_-\rangle=-\sqrt{\frac{2}{3}}\frac{\mu_B\zeta}{\Delta E'_{dq}},$$
$$\langle {}^2T_{1g}1/2a_0|\overline{\overline{P}}_x|{}^4A_{2g}3/2\rangle=\frac{1}{12}\frac{\zeta\langle {}^4T_{2g}\|\overline{P}_x[T_1]\|{}^4A_{2g}\rangle}{\Delta E'_{dq}},$$
$$\langle {}^2T_{1g}1/2a_-|\overline{\overline{P}}_x|{}^4A_{2g}3/2\rangle=\frac{1}{6}\frac{\zeta\langle {}^4T_{2g}\|\overline{P}_x[T_1]\|{}^4A_{2g}\rangle}{\Delta E'_{dq}}, \quad (3.28)$$

with $\Delta E'_{dq}=E({}^2T_{1g})-E({}^4T_{2g})$. We have another channel giving rise to the real electric-dipole transition to the state $|{}^2T_{1g}1/2a_0\rangle$ through the state $|{}^4T_{1g}3/2a_-\rangle$. To evaluate this effective electric-dipole moment, we use Eq. (3.6) and the following spin-orbit interaction:

$$\langle {}^2T_{1g}1/2a_0|\mathcal{H}_{\rm so}|{}^4T_{1g}3/2a_-\rangle$$
$$=-\langle {}^2T_{1g}\|V_{\rm so}\|{}^4T_{1g}\rangle\frac{1}{\sqrt{2}}\frac{1}{\sqrt{3}}\left\langle\frac{1}{2}\frac{1}{2}\middle|\frac{3}{2}\frac{3}{2}1-1\right\rangle$$
$$\times\langle T_1a_0|T_1a_-T_1a_+\rangle$$
$$=3\sqrt{2}i\zeta\frac{1}{\sqrt{6}}\frac{1}{\sqrt{2}}\frac{i}{\sqrt{2}}=-\frac{\sqrt{3}}{2}\zeta. \quad (3.29)$$

This channel also gives the real electric dipole as

$$\langle {}^2T_{1g}1/2a_0|\overline{\overline{P}}_x|{}^4A_{2g}3/2\rangle=-\frac{\zeta}{4\sqrt{3}}\frac{\langle {}^4T_{1g}\|\overline{P}_x[T_2]\|{}^4A_{2g}\rangle}{\Delta E''_{dq}}, \quad (3.30)$$

where $\Delta E''_{dq}=E({}^2T_{1g})-E({}^4T_{1g})$. Then the magnetoelectric susceptibility $\alpha_{xx}^{(d)}(\omega)$ at ${}^2T_{1g}$ is evaluated at low temperatures as

$$\alpha_{xx}^{(d)}(\omega)=-A_0\left(\frac{\zeta}{2\sqrt{3}\Delta E'_{dq}}\right)^2$$
$$\times\left[\frac{4}{E({}^2T_{1g}1/2a_-)-E({}^4T_{2g}3/2)-\omega-i\Gamma_d}\right.$$
$$\left.+\frac{C-1}{E({}^2T_{1g}1/2a_0)-E({}^4T_{2g}3/2)-\omega-i\Gamma_d}\right], \quad (3.31)$$

where

$$C=\sqrt{3}\left(\frac{\Delta E'_{dq}}{\Delta E''_{dq}}\right)\frac{\langle {}^4T_{1g}\|\overline{P}_x[T_2]\|{}^4A_{2g}\rangle}{\langle {}^4T_{2g}\|\overline{P}_x[T_1]\|{}^4A_{2g}\rangle}.$$

The spin-orbit splitting within the multiplets ${}^2E_g$ and ${}^2T_{1g}$ vanishes for the configuration $(t_2)^3$. The energy splitting between $|{}^2T_{1g}1/2a_-\rangle$ and $|{}^2T_{1g}1/2a_0\rangle$ comes from the interplay between the spin-orbit interaction and the crystalline

field. Hybridization of the multiplet $|^4T_{1g}M_s a_m\rangle$ by the spin-orbit interaction can also be taken into account by

$$|^4T_{1g}3/2a_-^*\rangle=\alpha|3/2a_-\rangle+\beta|1/2a_0\rangle+\gamma|-1/2a_+\rangle, \tag{3.32}$$

with the same coefficients as Eq. (3.21). Then the state $|^2T_{1g}-1/2a_+\rangle$ can contribute to $\alpha_{xx}(\omega)$ with the same order of perturbations as for $|^2T_{1g}1/2a_-\rangle$. The magnetic-dipole moment $\bar{M}_x$ is evaluated as

$$\begin{aligned}\bar{M}_x&=\langle{}^4A_{2g}3/2|M_x|{}^4T_{2g}3/2x_-^*\rangle\\&\quad\times\frac{\langle{}^4T_{2g}3/2x_-^*|\mathcal{H}_{\rm so}|{}^2T_{1g}-1/2a_+\rangle}{E({}^2T_{1g}-1/2a_+)-E({}^4T_{2g}3/2x_-^*)}\\&=-\sqrt{\frac{2}{3}}\frac{\mu_B\zeta}{\Delta E'_{dq}}\left(\frac{\alpha\beta^*}{2\sqrt{6}}\right)\end{aligned} \tag{3.33}$$

and the electric-dipole moment is

$$\begin{aligned}\bar{\bar{P}}_x&=\frac{\langle{}^2T_{1g}-1/2a_+|\mathcal{H}_{\rm so}|{}^4T_{2g}3/2x_-^*\rangle}{E({}^2T_{1g}-1/2a_+)-E({}^4T_{2g}3/2x_-^*)}\\&\quad\times\langle{}^4T_{2g}3/2x_-^*|\bar{P}_x|{}^4A_{2g}3/2\rangle\\&\quad+\frac{\langle{}^2T_{1g}-1/2a_+|\mathcal{H}_{\rm so}|{}^4T_{1g}3/2a_-^*\rangle}{E({}^2T_{1g}-1/2a_+)-E({}^4T_{1g}3/2a_-^*)}\\&\quad\times\langle{}^4T_{1g}3/2a_-^*|\bar{P}_x|{}^4A_{2g}3/2\rangle\\&=-\frac{\alpha^*\beta\zeta}{12\sqrt{3}\Delta E'_{dq}}\langle{}^4T_{2g}\|\bar{P}_x[T_1]\|{}^4A_{2g}\rangle\\&\quad-\frac{\alpha^*\beta\zeta}{12\Delta E''_{dq}}\langle{}^4T_{1g}\|\bar{P}_x[T_2]\|{}^4A_{2g}\rangle.\end{aligned} \tag{3.34}$$

Therefore the magnetoelectric susceptibility at $|^2T_{1g}-1/2a_+\rangle$ is evaluated as follows:

$$\begin{aligned}\alpha_{xx}^{(d')}(\omega)&=A_0\left(\frac{\zeta}{2\sqrt{3}\Delta E'_{dq}}\right)^2\\&\quad\times\frac{R'}{E({}^2T_{1g}-1/2a_+)-E({}^4A_{2g}3/2)-\omega-i\Gamma_d},\end{aligned} \tag{3.35}$$

with $R'=|\alpha\beta^*|^2(1+C)/(24\sqrt{2})$ at sufficiently low temperatures. These magnetoelectric spectra are compared with the observed ones[8] in Sec. IV. These contributions are, however, also shown to vanish above the Néel temperature because the equal thermal distribution in the ground state $^4A_{2g}M_s=\pm3/2$ and $\pm1/2$ cancels out $\alpha_{xx}(\omega)$.

IV. COMPARISON WITH MAGNETOELECTRIC EXPERIMENTS

The theoretical results obtained in Sec. III are compared with the observed spectra of ellipticity and polarization rotation around the transition frequency to the ^2E_g, $^2T_{1g}$, and $^4T_{2g}$ states of Cr_2O_3 crystal in this section. We also predict these spectra at $^4T_{1g}$.

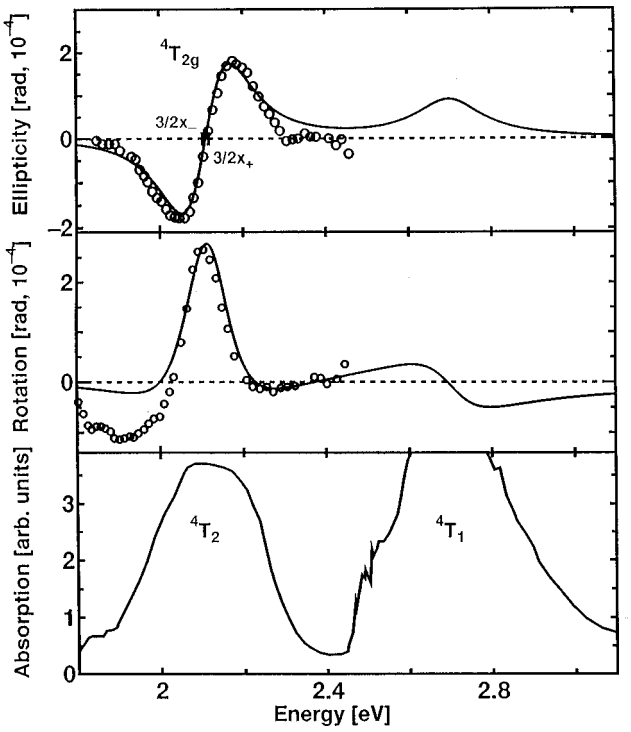

FIG. 2. The spectra of linear absorption (Ref. 13), polarization rotation, and ellipticity at the spin-allowed transitions $^4T_{2g}$ and $^4T_{1g}$. White circles describe the observed data (Ref. 8) and solid lines theoretical curves.

We start from the spectra at the spin-allowed transition at $^4T_{2g}$. Krichevtsov *et al.*[8] assigned the (positive) peak of ellipticity at 2.17 eV and (negative) bottom at 2.05 eV, respectively, to the absorptive-type spectrum of ellipticity due to the transitions to $^4T_{2g}x_\pm$ and $^4T_{2g}x_0$. Here they assumed the same magnitude of oscillator strengths and the opposite sign for these two transitions. However, both of these assumptions look very difficult to accept. These two characteristics, i.e., the positive ellipticity peak at 2.17 eV and the negative bottom at 2.05 eV with the same magnitude, can be explained very naturally in our model. The present model in fact gives us good agreement with the observed spectra of both ellipticity and rotation by using the material constants obtained from other experiments as has been shown in Fig. 2. We choose E^* in Eq. (3.10) at 90 K to be 2.12 eV, the splitting $E(^4T_{2g}3/2x_+)-E(^4T_{2g}3/2x_-)=3\lambda/2$ by the spin-orbit interaction to be 15 meV,[14] and the relaxation rate $\Gamma_a=0.1$eV.[13,21] The value $2A(n_\perp+1)/(n_\perp-1)$ is chosen as an adjustable parameter in drawing Fig. 2 and will be found to be reasonable from numerical estimation as will be shown below. The essential features of the observed spectra are well reproducible by these theoretical curves: (1) the positive peak on the high-energy side and the negative valley on the low side have the same absolute values and the opposite sign in the ellipticity spectrum at $^4T_{2g}$ and (2) the bell-shaped spectrum of rotation with negative signals on both tails, in agreement with both observed spectra. This comes from the fact that two levels of $^4T_{2g}x_\pm$ have the contribution to the magnetoelectric spectrum $\alpha_{xx}^{(a)}(\omega)$ with the same magnitude

but with the opposite sign as Eq. (3.10) shows. A small deviation of both tail parts may come from rather strong electron-phonon coupling,[21] as the present model is trying to describe this effect solely in terms of single relaxation constant Γ_a.

We will check the numerical magnitude of peak values θ_a and ϵ_a of the rotation and ellipticity spectra, $2A(n_\perp+1)/[\Gamma_a^2(n_\perp-1)]$. By using the number density of Cr^{3+} ions $4N=3.3\times10^{28}\ \mathrm{m}^{-3}$ and the effective electric-dipole moment $\overline{P_x}=0.9\times10^{-31}$ C m, $A/\Gamma_a^2=10^{-5}$, and $2A(n_\perp+1)/[\Gamma_a^2(n_\perp-1)]=10^{-4}$, in agreement with the observed value.[8] The effective dipole moment $\overline{P_x}$ is estimated as the atomic electric-dipole moment ea_0 ($a_0=$ Bohr radius) times $\langle V_{\mathrm{odd}}\rangle/\Delta E_o\approx0.1\mathrm{eV}/10\ \mathrm{eV}$.

The magnetoelectric spectrum at ${}^4T_{1g}$ is simplified at such a low temperature as $T\ll T_N=307.5$ K into the following form:

$$\alpha_{xx}^{(b)}(\omega)=-2B\left(M_s=\frac{3}{2}\right)\frac{1}{E^{**}-\omega-i\Gamma_b},\qquad(4.1)$$

where

$$E^{**}=\frac{1}{2}\sum_{\pm}\{E({}^4T_{1g}M_s a_\pm)-E({}^4A_{2g}M_s)\}.\qquad(4.2)$$

The spectra of ellipticity and rotation at ${}^4T_{1g}$ are of ordinary form, i.e., absorptive and dispersive, respectively, in contrast to those at ${}^4T_{2g}$. The maximum value $4B_0(n_\perp+1)/[\Gamma_b|\Delta E_1|(n_\perp-1)]$ of the polarization rotation θ_b and ellipticity ϵ_b at ${}^4T_{1g}$ is compared to that at ${}^4T_{2g}$, where $B_0(M_s)\equiv A_0\lambda M_s$. We also assumed that $\langle {}^4T_{1g}\|\overline{P_x}[T_2]\|{}^4A_{2g}\rangle$ has the same sign as $\langle {}^4T_{2g}\|\overline{P_x}[T_1]\|{}^4A_{2g}\rangle$. The relative magnitude $2\Gamma_a^2/(\Gamma_b|\Delta E_1|)$ is estimated to be about 1/3. We also assumed the refractive indices $n_\perp$ at ${}^4T_{2g}$ and ${}^4T_{1g}$ to be equal to each other and $\Gamma_b=\Gamma_a=0.1$ eV while the energy separation $|\Delta E_1|$ between ${}^4T_{1g}$ and ${}^4T_{2g}$ is 0.6 eV. The spectra of ellipticity and rotation are drawn in Fig. 2 by using these material constants.

Signals of spin-forbidden transitions at ${}^2E_g$ and ${}^2T_{1g}$ come from the higher-order perturbation of the spin-orbit interaction $\mathcal{H}_{\mathrm{so}}$ than the spin-allowed ones. The signal peaks at ${}^2E_g$ and ${}^2T_{1g}$, however, happen to be higher than that at ${}^4T_{2g}$ because the relaxation rates of ${}^2E_g$ and ${}^2T_{1g}$ levels are by two orders of magnitude smaller than that of ${}^4T_{2g}$ and ${}^4T_{1g}$. The latter are electronic transitions between the different configurations of ${}^4A_{2g}(t_2^3)$ and ${}^4T_{2g}(t_2^2e)$ or ${}^4T_{1g}(t_2^2e)$ so that they are broadened by the lattice vibration of the cubic field. On the other hand, the levels ${}^2E_g$ and ${}^2T_{1g}$ come from the same configuration as the ground state ${}^4A_{2g}$ so that they are almost free from the lattice vibration of the cubic field. As a result, these transitions are rather sharp. The magnetoelectric signals at $|{}^2E_g 1/2u_-\rangle$ and $|{}^2E_g-1/2u_+\rangle$ are dominant ones as calculated in Sec. III. The peak value at $|{}^2E_g 1/2u_-\rangle$ is $2A_0(\sqrt{2/3}\zeta/\Delta E'_{dq})^2(n'_\perp+1)/[\Gamma_c(n'_\perp-1)]$. As discussed above, the relaxation constant Γ_c is estimated to be 1 meV from the absorption spectrum and the magnetoelectric spectra.[8,13] The energy splitting $\Delta E'_{dq}=0.4$ eV between ${}^4T_{2g}$ and ${}^2E_g$ and the spin-orbit interaction $\zeta=3\lambda=30$ meV are used. The relative magnitude of signal peaks at ${}^2E_g$ to those at ${}^4T_{2g}$ is expressed by the product of two factors; $(4/9)[\Gamma_a^2/(\Gamma_c\lambda)](\sqrt{6}\lambda/\Delta E'_{dq})^2$ and $(n'_\perp+1)(n_\perp-1)/[(n'_\perp-1)(n_\perp+1)]$. The first factor is estimated to be of an order of unity. The data of refractive index $n_\perp$ at 2.1 eV and $n'_\perp$ at 1.7 eV are not available for the Cr_2O_3 crystal, but the second factor may be of an order of unity. Therefore the signal peaks at ${}^2E_g$ become of the same order of magnitude or a little larger than that at ${}^4T_{2g}$. When we choose a single parameter $(n'_\perp+1)(n_\perp-1)/[(n'_\perp-1)(n_\perp+1)]$ to be 2, i.e., $n'_\perp=2.1$ and $n_\perp=2.5$, the magnetoelectric spectra are drawn in good agreement with the observation[8] as shown in Fig. 3. The levels $|{}^2E_{1g}1/2u_-\rangle$ and $|{}^2E_{1g}-1/2u_+\rangle$ are split by the internal magnetic field $\mu_B H_i=24$ meV and located at 1.705 eV and 1.727 eV, respectively. The contributions to the magnetoelectric spectra from these levels have the opposite sign, as Eq. (3.19) and Eq. (3.24) show. The relative magnitude R is chosen to 0.2 to get the better fitting between the experimental and theoretical results although it is estimated to be of an order of 0.02 from Eq. (3.25). Here we used the spin-orbit interaction λ of an order of 10 meV, the internal field $\mu_B H_i$ about 20 meV at low temperature, and the trigonal crystalline field parameter K of an order of +30 meV. The relaxation rate Γ_c is chosen commonly to be 1 meV. Note that the ellipticities at ${}^2E_g 1/2u_-$ and ${}^2E_g-1/2u_+$ have opposite signs in agreement with observation[8] although the authors of Ref. 8 suspect that they should be of equal sign according to the theory developed in Refs. 22 and 23. As Fig. 3 shows, we have good agreement of the rotation spectrum between the experiment and the theory, but there remain two problems. The first is some positive background in the ellipticity spec-

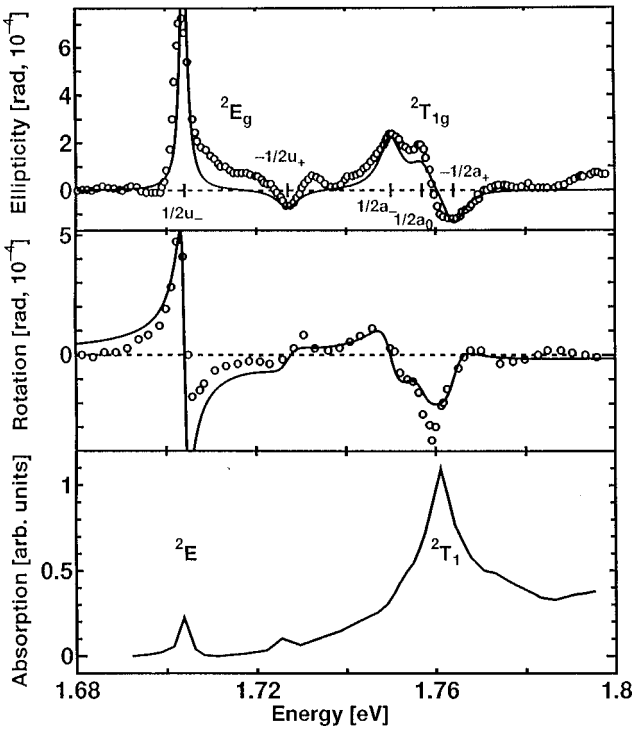

FIG. 3. The spectra of linear absorption (Ref. 13), polarization rotation, and ellipticity at the spin-forbidden transitions ${}^2E_g$ and ${}^2T_{1g}$. White circles from Ref. 8 and solid lines show theoretical results.

trum around $E(^2E_g-1/2u_+)=1.727$ eV. This may be related to the excitonic levels proposed by Macfarlane and co-workers.[22,23] The second problem is that the observed relative magnitude R of the signals at $|^2E_g 1/2u_-\rangle$ and $|^2E_g-1/2u_+\rangle$ is by one order of magnitude larger than the theoretical result Eq. (3.25). This may come from the uncertainty of material constants K, $\mu_B H_i$, and λ, and/or from the vibronic effect. In the present model, we have used the static model of crystalline field $V_{\rm trig}$. However, when the vibronic levels of the lattice vibration are taken into account, both the states $|^4T_{2g}x_0\rangle$ and $|^4T_{2g}x_\pm\rangle$ may become more strongly hybridized than in the static model. This will result in larger value of R. However, this problem is beyond the scope of the present treatment.

The three levels of the $^2T_{1g}$ manifold, i.e., $|^2T_{1g}1/2a_-\rangle$, $|^2T_{1g}1/2a_0\rangle$, and $|^2T_{1g}-1/2a_+\rangle$, contribute to the magnetoelectric spectra equally in the lowest-order perturbations of spin-orbit interaction and lower-symmetry crystalline field. The largest splitting in this manifold comes from the internal magnetic field, which results in the splitting of an order of $\mu_B H_i=24$meV. The splitting between $|^2T_{1g}1/2a_0\rangle$ and $|^2T_{1g}1/2a_-\rangle$ is due to the combined effect of $\mathcal{H}_{\rm so}$ and $V_{\rm trig}$. We have assigned these levels $|^2T_{1g}1/2a_-\rangle$, $|^2T_{1g}1/2a_0\rangle$ and $|^2T_{1g}-1/2a_+\rangle$ at 1.75 eV, 1.757 eV, and 1.764 eV in this order. Although the largest observed splitting 14 meV is a little smaller than the value 24 meV expected theoretically, the calculated magnetoelectric spectra seem to be in good agreement with observed ones as Fig. 3 shows. Here C in Eq. (3.31) and R' in Eq. (3.35) are chosen to be 3 and 4, respectively. The value of C looks reasonable from $\langle ^4T_{1g}||\overline{P}_x[T_2]||^4A_{2g}\rangle/\langle ^4T_{2g}||\overline{P}_x[T_1]||^4A_{2g}\rangle\simeq\sqrt{3}$ and $(\Delta E'_{dq}/\Delta E''_{dq})\simeq 1$. However, we have the same problem for the value R' as for R. Also in this case, we have to assume strong dynamical coupling between $|^4T_{1g}a_\pm\rangle$ and $|^4T_{1g}a_0\rangle$ in Eq. (3.32) as for Eq. (3.21).

V. SHG SPECTRA

The purpose of the present section is to evaluate explicitly the nonvanishing expressions of χ^m and χ^e and to see if they are able to explain the observed magnitudes of the susceptibilities and the interference effect.

We first calculate the dominant contributions to χ^m and χ^e which contain the resonant denominator of signal frequency 2ω nearly equal to the excitation frequency from $^4A_{2g}$ to $^4T_{2g}x_\pm$ or $^4T_{2g}x_0$ states.

During these calculations, we are able to confirm that both χ^m and χ^e for the crystal vanish under the C_{3v} symmetry around Cr^{3+} ions even though those for a single site do not. This was proved in a previous paper[12] by using group theory. As emphasized there, this is true even when we evaluate χ^m and χ^e by taking account of perturbations of $V_{{\rm axial},g}$, $V_{{\rm axial},u}$, and $\mathcal{H}_{\rm so}$, to the higher orders. As long as only the conventional trigonal crystalline field, i.e., $V_{\rm axial}$, is taken into account as perturbation on the trigonal bases, the finite contributions to χ^m and χ^e at each of the four sites in the unit cell turn out to be real to any order of perturbations. Summing up the four contributions from A_1, B_1, B_2, and A_2 sites, which are calculated by using Eqs. (2.1)–(2.3), χ^m and χ^e are found then to vanish without exception. This is in agreement with Eqs. (2.30) and (2.31), because these equations describe that only the imaginary part of (MPP) and $(\overline{P}PP)$ can contribute to χ^m and χ^e, which implies that $V_{\rm twist}$ has to be included at least once in the perturbed expressions of (MPP) and $(\overline{P}PP)$ to make them imaginary. In the present paper, this fact will be verified in the Appendix by calculating the relevant (reduced) matrix elements explicitly.

A. Magnetic susceptibility

Let us start from χ^m of Eq. (2.30). We are interested only in the term where $|m\rangle=|^4T_{2g}x_m\rangle$ and $|i\rangle=|^4A_{2g}\rangle$. The perturbed eigenfunctions ϕ_j may be expressed in terms of the unperturbed basis functions ψ_j as

$$\phi_j=\psi_j+\sum_{j'}\psi_{j'}\frac{(\mathcal{H}')_{j'j}}{\Delta E(jj')}. \tag{5.1}$$

We have four possible cases leading to finite matrix elements of magnetic-dipole moment M_x, i.e., (1) $M_{im}\neq 0$, (2) $M_{im'}\neq 0$, (3) $M_{i'm}\neq 0$, and (4) $M_{i'm'}\neq 0$ for the unperturbed i and perturbed i' ground states. The magnetic-dipole moment $\boldsymbol{M}$ is the sum of angular momentum $\boldsymbol{L}$ and spin operator $\boldsymbol{S}$, that is, $\boldsymbol{M}=-\mu_B(\boldsymbol{L}+2\boldsymbol{S})$ with μ_B the Bohr magneton. In the first case, which results in the dominant contribution to χ^m, the magnetic-dipole moment M_x connects the excited states $^4T_{2g}x_m$ to the ground state $^4A_{2g}$ through the matrix elements given by Eq. (3.1). Remember that the states $^4T_{2g}x_m$ cannot be excited directly through the two-photon process from the ground state $^4A_{2g}$.[24] One possibility is the indirect excitation via the states $^4T_{1g}a_m$ which are closest to them and linked by the field $V_{{\rm twist},g}$. The other is the mixing of the state $^4T_{2g}x_0$ with $^4A_{2g}$ due to this field. This also makes the two-photon excitation to $^4T_{2g}x_m$ possible.

The corresponding term (χ^m per single ion at A_1 site) apart from the constant factor $n/\epsilon_0 c$ is denoted as $\chi^m_{(1)}$ and evaluated as

$$\chi^m_{(1)}=-\frac{\mu_B}{2}\times\sum_{M_s,m=\pm}\frac{\langle ^4A_{2g}M_s|L_{-m}|^4T_{2g}M_s x_m\rangle C_m\rho_0(M_s)}{E(^4T_{2g}M_s x_m)-E(^4A_{2g}M_s)-2\hbar\omega-i\Gamma_m}, \tag{5.2}$$

where

$$C_m=\sum_{n,k}\frac{\langle ^4T_{2g}M_s x_m|V_{{\rm twist},g}|n\rangle}{E(^4T_{2g}M_s x_m)-E(n)}\frac{\langle n|P_x|k\rangle\langle k|P_x|^4A_{2g}M_s\rangle}{E(k)-E(^4A_{2g}M_s)-\hbar\omega}+\sum_k\frac{\langle ^4T_{2g}M_s x_m|P_x|k\rangle\langle k|P_x|^4T_{2g}M_s x_0\rangle}{E(k)-E(^4A_{2g}M_s)-\hbar\omega}\times\frac{\langle ^4T_{2g}M_s x_0|V_{{\rm twist,g}}|^4A_{2g}M_s\rangle}{E(^4A_{2g}M_s)-E(^4T_{2g}M_s x_0)}. \tag{5.3}$$

In accordance with the causality requirement, we have introduced the rates $\Gamma_m(m=\pm 1,0)$ to take account of the relax-

ation of the excited states ${}^4T_{2g}x_m(m=\pm1,0)$, as we want to discuss the resonant second-harmonic generation between the ground state ${}^4A_{2g}$ and the excited state ${}^4T_{2g}x_m(m=\pm1,0)$.

As mentioned above, we should choose only the states ${}^4T_{1g}a_m$ as the intermediate state $|n\rangle$, because the denominator of the first factor in Eq. (5.3) then becomes smallest among the possible states. But then, it turns out that the matrix element $\langle {}^4T_{2g}M_s x_m|V_{\text{twist},g}|{}^4T_{1g}a_m\rangle$ vanishes within the present (strong field) approximation as shown in the Appendix, so that only the second sum of Eq. (5.3) will be considered hereafter.

The two-photon excitation process in Eq. (5.3) is evaluated by using the closure approximation as follows:

$$\sum_k \frac{P_x|k\rangle\langle k|P_x}{E(k)-E({}^4A_{2g}M_s)-\hbar\omega}=\frac{P_x^2}{\Delta E_o}, \tag{5.4}$$

where ΔE_o is the energy separation between $4p$ and $3d$ states of the Cr^{3+} ion. The dipole moment operator P_x is then expressed in terms of the operator of type $T_1a_\pm: a_\pm=\mp(P_x\pm iP_y)/\sqrt{2}$. This makes it possible to decompose the square

$$P_x^2=\frac{1}{2}\{a_+^2+a_-^2-(a_+a_-+a_-a_+)\} \tag{5.5}$$

into its irreducible components by using tables of the Clebsch-Gordan coefficients for $T_1\times T_1$.[15] Thus P_x^2 is decomposed as

$$P_x^2=\frac{1}{\sqrt{6}}\sum_{m=\pm} mP_x^2[T_2x_m]+\frac{1}{\sqrt{6}}P_x^2[T_2x_0] + \frac{1}{2\sqrt{3}}\sum_{m=\pm} mP_x^2[Eu_m]-\frac{1}{\sqrt{3}}P_x^2[A_1]. \tag{5.6}$$

For example, the components with the symmetry $T_2x_\pm$ and $Eu_\pm$ are given by

$$P_x^2[T_2x_\pm]=\sum_{m,m'} a_m a_{m'}\langle T_1a_mT_1a_{m'}|T_2x_\pm\rangle = \frac{1}{\sqrt{6}}(a_\pm a_0+a_0a_\pm\pm 2a_\mp a_\mp), \tag{5.7}$$

$$P_x^2[Eu_\pm]=-\frac{1}{\sqrt{3}}(a_\pm a_0+a_0a_\pm\mp a_\mp a_\mp), \tag{5.8}$$

where $a_0=P_z$ belongs to the representation T_1a_0.

The matrix elements in Eq. (5.3) can now be evaluated in terms of the reduced matrix elements by using the Wigner-Eckart theorem:

$$\langle {}^4T_{2g}M_s x_m|P_x^2|{}^4T_{2g}M_s x_0\rangle = \frac{m}{\sqrt{6}}\left\langle {}^4T_{2g}M_s x_m\middle| P_x^2[T_2x_m] + \frac{1}{\sqrt{2}}P_x^2[Eu_m]\middle|{}^4T_{2g}M_s x_0\right\rangle = -\frac{m}{6\sqrt{3}}\left(\langle {}^4T_{2g}\|P_x^2[T_2]\|{}^4T_{2g}\rangle - \sqrt{\frac{3}{2}}\langle {}^4T_{2g}\|P_x^2[E]\|{}^4T_{2g}\rangle\right), \tag{5.9}$$

$$\langle {}^4T_{2g}M_s x_m|V_{\text{twist},g}[T_1a_0]|{}^4A_{2g}M_s\rangle = \frac{1}{\sqrt{3}}\langle {}^4T_{2g}\|V_{\text{twist},g}[T_1]\|{}^4A_{2g}\rangle. \tag{5.10}$$

Now the expression of C_m [Eq. (5.3)] is simplified into the following form:

$$C_m=-\frac{m}{18}\frac{\langle {}^4T_{2g}\|P_x^2[T_2]\|{}^4T_{2g}\rangle-\sqrt{3/2}\langle {}^4T_{2g}\|P_x^2[E]\|{}^4T_{2g}\rangle}{\Delta E_o} \times\frac{\langle {}^4T_{2g}\|V_{\text{twist},g}[T_1]\|{}^4A_{2g}\rangle}{\Delta E_2}, \tag{5.11}$$

with the energy difference ΔE_2 defined by

$$\Delta E_2=E({}^4A_{2g}M_s)-E({}^4T_{2g}M_s x_0). \tag{5.12}$$

Summing up these results, we obtain

$$\chi_{(1)}^m=\sum_{M_s,m}\frac{iA^m\rho_0(M_s)}{E({}^4T_{2g}M_s x_m)-E({}^4A_{2g}M_s)-2\hbar\omega-i\Gamma_m}, \tag{5.13}$$

with

$$A^m=\sqrt{2}\mu_B m C_m, \tag{5.14}$$

where $\rho_0(M_s)\equiv\rho({}^4A_{2g}M_s)=\rho_i$ in Eq. (2.30). At 0 K and at the site A_1, the spin distribution $\rho_0(M_s)$ is chosen to be unity for $M_s=3/2$ and zero otherwise.

The second contribution $\chi_{(2)}^m$ comes from case (2) $M_{im'}\neq0$ and (3) $M_{i'm}\neq0$. For case (2), we can choose the states $|m'\rangle=|{}^4T_{2g}M_s x_n\rangle(n=\pm1)$ which are connected to the state $|m\rangle=|{}^4T_{2g}M_s+nx_0\rangle$ by the off-diagonal components of the spin-orbit interaction:

$$|m\rangle_{\text{pert}}=|m\rangle+\sum_{m'}\frac{|m'\rangle\langle m'|\mathcal{H}_{\text{so}}|m\rangle}{\Delta E(mm')} =|m\rangle+\sum_{n=\pm}|{}^4T_{2g}M_s x_n\rangle \times\frac{\langle {}^4T_{2g}M_s x_n|\mathcal{H}_{\text{so}}^{-nn}|{}^4T_{2g}M_s+nx_0\rangle}{E({}^4T_{2g}M_s+nx_0)-E({}^4T_{2g}M_s x_n)}, \tag{5.15}$$

where $|m\rangle_{\rm pert} \equiv \psi_m$. Note that the spin-orbit interaction here has been decomposed as follows:

$$\mathcal{H}_{\rm so} = \sum_{n=\pm} \mathcal{H}_{\rm so}^{-nn} + \mathcal{H}_{\rm so}^{z} = \frac{\lambda}{2} \sum_{n=\pm} S_{-n} L_n + \lambda S_z L_z . \tag{5.16}$$

Then the states $|m\rangle = |^4T_{2g} M_s + n x_0\rangle$ can emit the second harmonics 2ω by the magnetic-dipole moment M_x. Compared with Eq. (5.15), we can show the contribution from case (3) $M_{i'm} \neq 0$ is negligible because of the large denominator involved. The ground state $|i\rangle = |^4A_{2g} M_s\rangle$ is modified only slightly by $\mathcal{H}_{\rm so}$.

Now we can write down the expression of $\chi_{(2)}^m$ in a simple way:

$$\chi_{(2)}^m = \sum_m \sum_{m_1, m_2} \frac{\langle i|M_x|m_1\rangle\langle m_1|\mathcal{H}_{\rm so}|m\rangle\langle m|\mathcal{H}_{\rm so}|m_2\rangle\langle m_2|P_x^2 V_{{\rm twist},g}|i\rangle}{\Delta E(mm_1)\{E(m) - 2\hbar\omega - i\Gamma_m\}\Delta E(mm_2)\Delta E_2 \Delta E_o}. \tag{5.17}$$

In this equation the first term $\langle i|M_x|m_1\rangle$ is the same as that in case (1) [Eq. (3.1)] and the last factor $\langle m_2|P_x^2 V_{{\rm twist},g}|i\rangle/\Delta E_2 \Delta E_o$ is equal to C_n [Eq. (5.3) or (5.11)] as $|m_2\rangle = |^4T_{2g} M_s x_n\rangle$. Inserting these into Eq. (5.17) we have

$$\begin{aligned}
\chi_{(2)}^m &= -\frac{\mu_B}{2} \sum_{M_s, n=\pm} C_n \rho_0(M_s) \frac{\langle {}^4A_{2g} M_s|L_{-n}|{}^4T_{2g} M_s x_n\rangle}{E({}^4T_{2g} M_s + n x_0) - E({}^4T_{2g} M_s x_n)} \frac{\langle {}^4T_{2g} M_s x_n|\mathcal{H}_{\rm so}^{-nn}|{}^4T_{2g} M_s + n x_0\rangle}{E({}^4T_{2g} M_s + n x_0) - E({}^4A_{2g} M_s) - 2\hbar\omega - i\Gamma_0} \\
&\quad \times \frac{\langle {}^4T_{2g} M_s + n x_0|\mathcal{H}_{\rm so}^{n-n}|{}^4T_{2g} M_s x_n\rangle}{E({}^4T_{2g} M_s + n x_0) - E({}^4T_{2g} M_s x_n)} \\
&= \frac{\lambda^2}{4} \sum_{M_s, n=\pm} \frac{\sqrt{2} n \mu_B i C_n \rho_0(M_s)}{E({}^4T_{2g} M_s + n x_0) - E({}^4A_{2g} M_s) - 2\omega - i\Gamma_0} \left| \frac{\langle {}^4T_{2g} M_s x_n|S_{-n} L_n|{}^4T_{2g} M_s + n x_0\rangle}{E({}^4T_{2g} M_s + n x_0) - E({}^4T_{2g} M_s x_n)} \right|^2 \\
&= \frac{\lambda^2}{8} \sum_{M_s, n=\pm} \frac{i A^m \rho_0(M_s)}{E({}^4T_{2g} M_s + n x_0) - E({}^4A_{2g} M_s) - 2\hbar\omega - i\Gamma_0} \left| \frac{S(S+1) - M_s(M_s+n)}{E({}^4T_{2g} M_s + n x_0) - E({}^4T_{2g} M_s x_n)} \right|^2 .
\end{aligned} \tag{5.18}$$

Remembering

$$\langle M_s|S_{-n}|M_s + n\rangle = \sqrt{S(S+1) - M_s(M_s+n)}, \tag{5.19}$$

and using

$$\langle {}^4T_{2g} x_n|L_n|{}^4T_{2g} x_0\rangle = 1/\sqrt{2} \quad (n = \pm), \tag{5.20}$$

we find that $\chi_{(2)}^m$ may be written as

$$\chi_{(2)}^m = \sum_{M_s, n=\pm} \frac{i B^m \rho_0(M_s)}{E({}^4T_{2g} M_s + n x_0) - E({}^4A_{2g} M_s) - 2\hbar\omega - i\Gamma_0}. \tag{5.21}$$

At 0 K and at the site A_1, $M_s = 3/2$ is dominantly populated [the same as in case (1)] and the only state $|^4T_{2g} M_s = 1/2 x_0\rangle (n = -1)$ will contribute finitely to $\chi_{(2)}^m$. The relative magnitude of $\chi_{(2)}^m$ to $\chi_{(1)}^m$ may be estimated from

$$B^m = \frac{3}{8} \left(\frac{\lambda}{\Delta E_3} \right)^2 A^m, \tag{5.22}$$

with

$$\Delta E_3 \equiv E\left({}^4T_{2g} \frac{1}{2} x_0 \right) - E\left({}^4T_{2g} \frac{3}{2} x_- \right), \tag{5.23}$$

where

$$|\Delta E_3| = |\Delta E - \mu_B H_i - 3\lambda/4| \sim 65 \ \text{meV}, \tag{5.24}$$

by Eqs. (2.15) and (2.16) and $\lambda \sim 10$ meV.

So far we have calculated the contribution of a particular single channel to $\chi_{(2)}^m$, i.e., the term with the numerator

$$\langle i|M_x \mathcal{H}_{\rm so}|m\rangle\langle m|\mathcal{H}_{\rm so} P_x P_x V_{{\rm twist},g}|i\rangle. \tag{5.25}$$

There are, however, 12 similar terms to this order of perturbation which can give rise to the same resonance effect at $|m\rangle = |^4T_{2g} M_s = 1/2 x_0\rangle$ in the SHG. This is because we have 12 possibilities to put $\mathcal{H}_{\rm so}$ and $V_{{\rm twist},g}$ in the second factor of Eq. (5.25). We cannot evaluate numerically all of these terms at present because of the poor information available to us on the highly excited intermediate states (especially those of odd parity). This point will be taken into consideration again in Sec. VI.

The matrix elements in C_m [in Eq. (5.3) or (5.11)] can be evaluated using the many-electron wave functions given in the Appendix. It then turns out that C_m is real. As a result both $\chi_{(1)}^m$ and $\chi_{(2)}^m$ are pure imaginary under off-resonant condition so that both remain finite after summing up the contributions from four Cr^{3+} ions in a unit cell, in accordance with Eqs. (2.28) and (2.30).

The total susceptibility $\chi_{\rm total}^m$ is written down with the Cr^{3+} ion density $4N$ as

$$\chi^m_{\text{total}}=\frac{4Nn}{\epsilon_0 c}(\chi^m_{(1)}+\chi^m_{(2)}). \tag{5.26}$$

B. Electric susceptibility

The second-order susceptibilities due to electric-dipole moment χ^e_{total} are nonvanishing only below Néel temperature T_N where the crystal Cr_2O_3 loses the inversion symmetry. We list microscopic mechanisms for χ^e given by Eq. (2.31) with 2ω resonant to the transition between the ground state ${}^4A_{2g}$ and the excited states ${}^4T_{2g}$. These are required to lead not only to a nonvanishing value of the susceptibility for a single Cr^{3+} ion, but also to a finite value of χ^e_{total} even after the susceptibilities have been summed up over the four different sites in the unit cell.

Two-photon excitation through a product of two electric-dipole moment operators P_x is possible only to the states ${}^4T_{1g}a_m$ from the ground state ${}^4A_{2g}$.[24] The spin-orbit interaction $\mathcal{H}^z_{\text{so}}=\lambda S_z L_z$ then mixes them with the states ${}^4T_{2g}x_m$. The latter states $|m\rangle=|{}^4T_{2g}M_s x_m\rangle$ are brought down to the ground state by the combined action of the electric-dipole moment P_x and the crystalline field of odd parity $V_{\text{twist},u}=V[T_{2u}x_0]$. In this section, we keep the same notation $\overline{P}_x$ as before for this effective dipole moment and define it also by Eq. (3.3), but with V_{odd} now replaced by $V_{\text{twist},u}$. The operator $\overline{P}_x$ may be decomposed in its irreducible components as

$$\overline{P}_x=\frac{i}{\sqrt{6}}\sum_{m=\pm}\overline{P}_x[Eu_m]+\frac{1}{2\sqrt{3}}\sum_{m=\pm}m\overline{P}_x[T_1a_m]+\frac{i}{2}\sum_{m=\pm}\overline{P}_x[T_2x_m]. \tag{5.27}$$

This is possible with the help of the Clebsch-Gordan coefficients for the product of $T_{1u}a_\pm$ and $T_{2u}x_0$ as in Eq. (5.6).[15] Note that the decomposition is quite different from the one in Eq. (3.4), because it is $V_{\text{twist},u}$ here that helps the electric-dipole transition.

Using this $\overline{P}_x$, the first contribution to the electric susceptibility per single ion, $\chi^e_{(1)}$, is evaluated apart from the factor $1/\epsilon_0$ as

$$\begin{aligned}\chi^e_{(1)}&=\sum_{M_s,m=\pm}\frac{\langle{}^4A_{2g}M_s|\overline{P}_x|{}^4T_{2g}M_s x_m\rangle}{E({}^4T_{2g}M_s x_m)-E({}^4A_{2g}M_s)-2\hbar\omega-i\Gamma_m}\\&\times\frac{\langle{}^4T_{2g}M_s x_m|\mathcal{H}^z_{\text{so}}|{}^4T_{1g}M_s a_m\rangle}{E({}^4T_{2g}M_s x_m)-E({}^4T_{1g}M_s a_m)}\\&\times\frac{\langle{}^4T_{1g}M_s a_m|P_x^2|{}^4A_{2g}M_s\rangle}{\Delta E_o}\rho_0(M_s)\\&=\sum_{M_s,m=\pm}\frac{iA^eM_s\rho_0(M_s)}{E({}^4T_{2g}M_s x_m)-E({}^4A_{2g}M_s)-2\hbar\omega-i\Gamma_m},\end{aligned} \tag{5.28}$$

where

$$A^e=\frac{\lambda}{36\sqrt{2}\Delta E_1\Delta E_o}\langle{}^4A_{2g}\|\overline{P}_x[T_1]\|{}^4T_{2g}\rangle\times\langle{}^4T_{1g}\|P_x^2[T_2]\|{}^4A_{2g}\rangle, \tag{5.29}$$

with ΔE_1 given by Eq. (3.8). In deriving this equation, we have used Eq. (5.9), the Wigner-Eckart theorem for $\overline{P}_x$ and the matrix element of $\mathcal{H}^z_{\text{so}}$ calculated by means of the wave functions given in the Appendix. For example, we find

$$\begin{aligned}&\langle{}^4A_{2g}M_s|\overline{P}_x|{}^4T_{2g}M_s x_m\rangle\\&\quad=-\frac{m}{2\sqrt{3}}\langle{}^4A_{2g}M_s|\overline{P}_x[T_1a_{-m}]|{}^4T_{2g}M_s x_m\rangle\\&\quad=-\frac{m}{6}\langle{}^4A_{2g}\|\overline{P}_x[T_1]\|{}^4T_{2g}\rangle,\end{aligned} \tag{5.30}$$

and

$$\langle{}^4T_{2g}M_s x_m|L_z|{}^4T_{1g}M_s a_m\rangle=\frac{i}{2}. \tag{5.31}$$

It is possible to show that the matrix elements of Eq. (5.9) and Eq. (5.29) are real by using the many-electron wave functions. As a consequence, A^e becomes real and $\chi^e_{(1)}$ is pure imaginary under off resonance.

It is in order here to comment on the relation between the present treatment and that of Muthukumar, Valenti, and Gros.[11] These authors proposed a microscopic theory to explain the observed nonreciprocal effect assuming the $(CrO_6)_2$ cluster model with D_{3d} symmetry. In their model, the ion at site A_1 is carried into the one at site B_2 with its surrounding environment by the twofold rotation. However, we find that the covering operation for the cluster in the real crystal is the inversion accompanied with the time reversal. Along with this, conventional trigonal crystalline fields with even and odd symmetry and spin-orbit interaction were considered in their treatment as perturbation on the trigonal states of the Cr^{3+} ion. Within their model, they were able to show that the spin-orbit interaction will lead to a linear dependence of χ^e on the sublattice magnetization. It is, however, unfortunate that they did not take the effect of magnetic symmetry into account correctly. As shown in our previous paper,[12] the correct symmetry leads to the result that both χ^m and χ^e vanish below T_N with the conventional crystalline fields when the contributions from the four Cr^{3+} ions in a unit cell are summed up, even though each single-site contribution to χ^m or χ^e does not. In order to obtain nonvanishing nonlinear susceptibilities, twisted crystalline fields around the Cr^{3+} ion have to be introduced. Apart from this, their result agrees with our $\chi^e_{(1)}$ in Eq. (5.28) except for the imaginary factor in the numerator, when the Zeeman energies in the molecular field which appear in the energy denominators are neglected.

The second contribution $\chi^{e}_{(2n)}$ corresponds to the second harmonic resonant to the transition between the ground state and the excited state $^4T_{2g}x_0$. In this case the electric-dipole transition becomes possible in association with the odd parity twisted crystalline field $V_{\text{twist},u}$ and the spin-orbit interaction $\mathcal{H}_{\text{so}}$, the intermediate state m_1 being modified by the spin-orbit interaction [Eq. (5.15)]. The channel is similar to that considered for $\chi^{m}_{(2)}$, involving $\mathcal{H}_{\text{so}}$ twice but without $V_{\text{twist},g}$. This time we can obtain a finite value without introducing $\mathcal{H}^{z}_{\text{so}}$ as in $\chi^{e}_{(1)}$, so that $\chi^{e}_{(2n)}$ can be simply written as

$$\chi^{e}_{(2n)}=\sum_{m}\sum_{m_1,m_2}\frac{\langle i|\overline{P_x}|m_1\rangle\langle m_1|\mathcal{H}_{\text{so}}|m\rangle\langle m|\mathcal{H}_{\text{so}}|m_2\rangle\langle m_2|P_x^2|i\rangle}{\Delta E(mm_1)\{E(m)-2\hbar\omega-i\Gamma_m\}\Delta E(mm_2)\Delta E_o}. \tag{5.32}$$

Then we evaluate this as follows:

$$\begin{aligned}
\chi^{e}_{(2n)}=&\sum_{M_s,m=\pm}\rho_0(M_s)\left(\frac{\langle {}^4A_{2g}M_s|\overline{P_x}|{}^4T_{2g}M_sx_m\rangle\langle {}^4T_{2g}M_sx_m|\mathcal{H}_{\text{so}}^{-mm}|{}^4T_{2g}M_s+mx_0\rangle}{E({}^4T_{2g}M_s+mx_0)-E({}^4T_{2g}M_sx_m)}\right.\\
&\left.+\frac{\langle {}^4A_{2g}M_s|\overline{P_x}|{}^4T_{1g}M_sa_m\rangle\langle {}^4T_{1g}M_sa_m|\mathcal{H}_{\text{so}}^{-mm}|{}^4T_{2g}M_s+mx_0\rangle}{E({}^4T_{2g}M_s+mx_0)-E({}^4T_{1g}M_sa_m)}\right)\frac{\langle {}^4T_{2g}M_s+mx_0|\mathcal{H}_{\text{so}}^{m-m}|{}^4T_{1g}M_sa_m\rangle}{E({}^4T_{2g}M_s+mx_0)-E({}^4A_{2g}M_s)-2\hbar\omega-i\Gamma_0}\\
&\times\frac{\langle {}^4T_{1g}M_sa_m|P_x^2|{}^4A_{2g}M_s\rangle}{[E({}^4T_{2g}M_s+mx_0)-E({}^4T_{1g}M_sa_m)]\Delta E_o}\\
=&\sum_{M_s,m=\pm}\rho_0(M_s)\left(\frac{\lambda}{2}\right)^2\{S(S+1)-M_s(M_s+m)\}\left(\frac{(-m/6)\langle {}^4A_{2g}\|\overline{P_x}[T_1]\|{}^4T_{2g}\rangle\times(1/\sqrt{2})}{\Delta E_3}\right.\\
&\left.+\frac{(i/2\sqrt{3})\langle {}^4A_{2g}\|\overline{P_x}[T_2]\|{}^4T_{1g}\rangle\times(im/\sqrt{2})}{\Delta E_4}\right)\frac{(-im/\sqrt{2})\times(-m/3\sqrt{2})\langle {}^4T_{1g}\|P_x^2[T_2]\|{}^4A_{2g}\rangle}{[E({}^4T_{2g}M_s+mx_0)-E({}^4A_{2g}M_s)-2\hbar\omega-i\Gamma_0]\Delta E_4\Delta E_o}\\
=&\sum_{M_s,m=\pm}\frac{(-i\sqrt{2}m\lambda^2/288)\{S(S+1)-M_s(M_s+m)\}\rho_0(M_s)}{E({}^4T_{2g}M_s+mx_0)-E({}^4A_{2g}M_s)-2\hbar\omega-i\Gamma_0}\left(\frac{\langle {}^4A_{2g}\|\overline{P_x}[T_1]\|{}^4T_{2g}\rangle}{\Delta E_3}+\frac{\sqrt{3}\langle {}^4A_{2g}\|\overline{P_x}[T_2]\|{}^4T_{1g}\rangle}{\Delta E_4}\right)\\
&\times\frac{\langle {}^4T_{1g}\|P_x^2[T_2]\|{}^4A_{2g}\rangle}{\Delta E_4\Delta E_o},
\end{aligned} \tag{5.33}$$

where we have made use of Eqs. (5.9), (5.19), (5.27),

$$\langle {}^4A_{2g}|\overline{P_x}|{}^4T_{1g}a_m\rangle=\frac{i}{2}\langle {}^4A_{2g}|\overline{P_x}[T_2x_{-m}]|{}^4T_{1g}a_m\rangle=\frac{i}{2\sqrt{3}}\langle {}^4A_{2g}\|\overline{P_x}[T_2]\|{}^4T_{1g}\rangle, \tag{5.34}$$

and

$$\langle {}^4T_{1g}a_m|L_m|{}^4T_{2g}x_0\rangle=im/\sqrt{2}, \tag{5.35}$$

as in Eqs. (5.30) and (5.31). The energy difference ΔE_4 here is defined by

$$\Delta E_4=E({}^4T_{2g}M_s+mx_0)-E({}^4T_{1g}M_sa_m). \tag{5.36}$$

At low temperatures, only the state $|{}^4A_{2g}M_s=3/2\rangle$ at the A_1 site is populated, so that the term with $m=-1$ will dominate on the right hand side of Eq. (5.33). As a result, $\chi^{e}_{(2n)}$ is simplified as

$$\chi^{e}_{(2n)}=\frac{iB^{e}_{n}}{E({}^4T_{2g}1/2x_0)-E({}^4A_{2g}3/2)-2\hbar\omega-i\Gamma_0}, \tag{5.37}$$

with

$$B^{e}_{n}=\frac{\sqrt{2}\lambda^2}{96}\left(\frac{\langle {}^4A_{2g}\|\overline{P_x}[T_1]\|{}^4T_{2g}\rangle}{\Delta E_3}+\frac{\sqrt{3}\langle {}^4A_{2g}\|\overline{P_x}[T_2]\|{}^4T_{1g}\rangle}{\Delta E_4}\right)\frac{\langle {}^4T_{1g}\|P_x^2[T_2]\|{}^4A_{2g}\rangle}{\Delta E_4\Delta E_o}. \tag{5.38}$$

We note here that $\Delta E_3 \equiv E(^4T_{2g}1/2x_0) - E(^4T_{2g}3/2x_-) \simeq -65$ meV and $\Delta E_4 \equiv E(^4T_{2g}1/2x_0) - E(^4T_{1g}3/2a_-) \simeq \Delta E_1 \equiv E(^4T_{2g}3/2x_m) - E(^4T_{1g}3/2a_m) \simeq -1$ eV. We may assume that $\langle {}^4A_{2g}\|\overline{P}_x[T_1]\|{}^4T_{2g}\rangle$ and $\langle {}^4A_{2g}\|\overline{P}_x[T_2]\|{}^4T_{1g}\rangle$ are of comparable magnitude, so that the relative magnitude will be given by $B_n^e/A^e \simeq 3\lambda/4|\Delta E_3| \sim 1/7$. Above $T > T_N$, this contribution vanishes as it should.

There is another contribution corresponding to the second harmonic resonant to the transition between the ground state and the excited state $^4T_{2g}x_0$. We call this second-order nonlinear susceptibility $\chi^e_{(2)}$ and evaluate it as follows:

$$\begin{aligned}
\chi^e_{(2)} &= \sum_{M_s,m=\pm} \rho_0(M_s) \left(\frac{\langle {}^4A_{2g}M_s|\overline{P}_x|{}^4T_{2g}M_s x_m\rangle \langle {}^4T_{2g}M_s x_m|\mathcal{H}_{\rm so}^{-mm}|{}^4T_{2g}M_s + mx_0\rangle}{E({}^4T_{2g}M_s + mx_0) - E({}^4T_{2g}M_s x_m)} \right. \\
&\quad \left. + \frac{\langle {}^4A_{2g}M_s|\overline{P}_x|{}^4T_{1g}M_s a_m\rangle \langle {}^4T_{1g}M_s a_m|\mathcal{H}_{\rm so}^{-mm}|{}^4T_{2g}M_s + mx_0\rangle}{E({}^4T_{2g}M_s + mx_0) - E({}^4T_{1g}M_s a_m)} \right) \frac{\langle {}^4T_{2g}M_s + mx_0|\mathcal{H}_{\rm so}^{m-m}|{}^4T_{2g}M_s x_m\rangle}{E({}^4T_{2g}M_s + mx_0) - E({}^4A_{2g}M_s) - 2\hbar\omega - i\Gamma_0} \\
&\quad \times \frac{\langle {}^4T_{2g}M_s x_m|\mathcal{H}_{\rm so}^{z}|{}^4T_{1g}M_s a_m\rangle}{E({}^4T_{2g}M_s + mx_0) - E({}^4T_{2g}M_s x_m)} \frac{\langle {}^4T_{1g}M_s a_m|P_x^2|{}^4A_{2g}M_s\rangle}{[E({}^4T_{2g}M_s x_m) - E({}^4T_{1g}M_s a_m)]\Delta E_o} \\
&= \sum_{M_s,m=\pm} \frac{\rho_0(M_s)(\lambda^2/4)\{S(S+1) - M_s(M_s+m)\}}{E({}^4T_{2g}M_s + mx_0) - E({}^4A_{2g}M_s) - 2\hbar\omega - i\Gamma_0} \left(\frac{(-m/6)\langle {}^4A_{2g}\|\overline{P}_x[T_1]\|{}^4T_{2g}\rangle \times (1/\sqrt{2})}{\Delta E_3} \right. \\
&\quad \left. + \frac{(i/2\sqrt{3})\langle {}^4A_{2g}\|\overline{P}_x[T_2]\|{}^4T_{1g}\rangle \times (im/\sqrt{2})}{\Delta E_4} \right) \frac{(1/\sqrt{2}) \times (i\lambda M_s/2) \times (-m/3\sqrt{2})\langle {}^4T_{1g}\|P_x^2[T_2]\|{}^4A_{2g}\rangle}{\Delta E_3 \Delta E_1 \Delta E_o} \\
&= i \sum_{M_s,m=\pm} \frac{B^e M_s \rho_0(M_s)}{E({}^4T_{2g}M_s + mx_0) - E({}^4A_{2g}M_s) - 2\hbar\omega - i\Gamma_0},
\end{aligned} \tag{5.39}$$

with

$$B^e = \frac{\lambda^3}{64\sqrt{2}} \left(\frac{\langle {}^4A_{2g}\|\overline{P}_x[T_1]\|{}^4T_{2g}\rangle}{\Delta E_3} + \frac{\sqrt{3}\langle {}^4A_{2g}\|\overline{P}_x[T_2]\|{}^4T_{1g}\rangle}{\Delta E_4} \right) \frac{\langle {}^4T_{1g}\|P_x^2[T_2]\|{}^4A_{2g}\rangle}{\Delta E_3 \Delta E_1 \Delta E_o} \tag{5.40}$$

using Eqs. (5.9), (5.19), (5.20), (5.30), (5.31), (5.34), and (5.35). From the perturbational point of view, this process is one order higher compared to $\chi^e_{(2n)}$. The relative magnitude of B^e to A^e of Eq. (5.29) is given by

$$B^e = \frac{3}{8} \left(\frac{\lambda}{\Delta E_3} \right)^2 A^e \sim 0.02. \tag{5.41}$$

Note that the remark made after Eq. (5.25) may apply here as well.

There is one more contribution to the susceptibility χ^e which leads to different intensities for the second harmonics generated from $^4T_{2g}x_+$ and $^4T_{2g}x_-$ contrary to $\chi^e_{(1)}$. This is obtained by replacing $\mathcal{H}^z_{\rm so}$ in Eq. (5.28) by the conventional trigonal field $V^c_{\rm trig}$ and is called $\chi^e_{(1a)}$:

$$\begin{aligned}
\chi^e_{(1a)} &= \sum_{M_s,m=\pm} \frac{\langle {}^4A_{2g}M_s|\overline{P}_x|{}^4T_{2g}M_s x_m\rangle}{E({}^4T_{2g}M_s x_m) - E({}^4A_{2g}M_s) - 2\hbar\omega - i\Gamma_m} \frac{\langle {}^4T_{2g}M_s x_m|V^c_{\rm trig}|{}^4T_{1g}M_s a_m\rangle}{E({}^4T_{2g}M_s x_m) - E({}^4T_{1g}M_s a_m)} \frac{\langle {}^4T_{1g}M_s a_m|P_x^2|{}^4A_{2g}M_s\rangle}{\Delta E_o} \rho_0(M_s) \\
&= \sum_{M_s,m=\pm} \frac{iC^e_a m \rho_0(M_s)}{E({}^4T_{2g}M_s x_m) - E({}^4A_{2g}M_s) - 2\hbar\omega - i\Gamma_m},
\end{aligned} \tag{5.42}$$

where

$$C^e_a = -\frac{\langle {}^4A_{2g}\|\overline{P}_x[T_1]\|{}^4T_{2g}\rangle}{36\sqrt{3}\Delta E_1 \Delta E_o} \langle {}^4T_{2g}\|V^c_{\rm trig}[T_2]\|{}^4T_{1g}\rangle \langle {}^4T_{1g}\|P_x^2[T_2]\|{}^4A_{2g}\rangle. \tag{5.43}$$

A similar contribution $\chi^e_{(1b)}$ follows if we replace $V_{{\rm twist},u}$ and $V_{{\rm axial},g}$ in the equations given above by $V_{{\rm axial},u} = V_{\rm odd}$ and $V_{{\rm twist},g}$, respectively:

$$\chi^e_{(1b)}=\sum_{M_s,m=\pm}\frac{\langle {}^4A_{2g}M_s|\overline{P^c_x}|{}^4T_{2g}M_sx_m\rangle}{E({}^4T_{2g}M_sx_m)-E({}^4A_{2g}M_s)-2\hbar\omega-i\Gamma_m}\frac{\langle {}^4T_{2g}M_sx_m|P^2_x|{}^4T_{2g}M_sx_0\rangle}{\Delta E_o}\frac{\langle {}^4T_{2g}M_sx_0|V_{\text{twist},g}|{}^4A_{2g}M_s\rangle}{E({}^4A_{2g}M_s)-E({}^4T_{2g}M_sx_0)}\rho_0(M_s)$$

$$=\sum_{M_s,m=\pm}\frac{iC^e_bm\rho_0(M_s)}{E({}^4T_{2g}M_sx_m)-E({}^4A_{2g}M_s)-2\hbar\omega-i\Gamma_m}, \tag{5.44}$$

where

$$C^e_b=\frac{1}{2\sqrt{3}}\langle {}^4A_{2g}\|\overline{P^c_x}[T_1]\|{}^4T_{2g}\rangle mC_m, \tag{5.45}$$

with C_m given by Eq. (5.11). The effective dipole moment $\overline{P^c_x}$ is well known in the interpretation of the absorption spectra of ruby,[15] and originates from the transition moment perturbed by $V_{\text{axial},u}\equiv V_{\text{odd}}$, which is exactly $\overline{P_x}$ employed in Sec. III. It is to be noted that both C^e_a and C^e_b may well be of the same order of magnitude as A^e of $\chi^e_{(1)}$, although $\chi^e_{(1a)}$ and $\chi^e_{(1b)}$ vanish because of the cancellation which occurs on the right hand sides of both Eqs. (5.42) and (5.44) when ${}^4T_{2g}x_+$ and ${}^4T_{2g}x_-$ have the same energy.

Finally, the expression for χ^e_{total} is given by

$$\chi^e_{\text{total}}=\frac{4N}{\epsilon_0}(\chi^e_{(1)}+\chi^e_{(2n)}+\chi^e_{(2)}+\chi^e_{(1a)}+\chi^e_{(1b)}). \tag{5.46}$$

C. Order estimation

In the present paper we neglect contributions of orders higher than those considered in the previous subsections. Estimation of the orders of magnitude of $|\chi^m|$ and $|\chi^e|$ around 2ω nearly equal to the excitation energy from the ground state ${}^4A_{2g}$ to the state ${}^4T_{2g}$ will now be the subject of this subsection. In general, $|\chi^e|$ is a few orders of magnitude larger than $|\chi^m|$. However, they are shown to be of the same order of magnitude in the present problem, because the χ^e process requires by one-order higher perturbation in the spin-orbit interaction $\mathcal{H}_{\text{so}}$ or the low-symmetry crystalline field V_{trig} for the transition in question. We are especially interested in the magnitudes of $\chi^m_{(1)}$ and $\chi^e_{(1)}$ which are supposed to be dominant in Eqs. (5.26) and (5.46), respectively.

First, we define ideal quantities of χ^m and χ^e in which all the matrix elements of M, $\overline{P}$, and P in Eqs. (2.30) and (2.31) take their nonvanishing unperturbed values, i.e.,

$$\chi^m_0=\frac{4Nn}{\epsilon_0c\hbar^2}M_{0m}\sum_k\frac{(PP)_{mk0}}{(\omega_m-2\omega)(\omega_k-\omega)}, \tag{5.47}$$

and

$$\chi^e_0=\frac{4N}{\epsilon_0\hbar^2}P_{0m}\sum_k\frac{(PP)_{mk0}}{(\omega_m-2\omega)(\omega_k-\omega)}. \tag{5.48}$$

As Eqs. (5.2) and (5.3) show, the absolute value of $|\chi^m_{(1)}|$ is reduced by a factor $\langle V_{\text{twist},g}\rangle/|\Delta E_2|$ compared to $|\chi^m_0|$, where $|\Delta E_2|\equiv E({}^4T_{2g})-E({}^4A_{2g})$, so that

$$|\chi^m_{(1)}|\sim|\chi^m_0|\frac{\langle V_{\text{twist},g}\rangle}{|\Delta E_2|}. \tag{5.49}$$

On the other hand, the electric susceptibility $\chi^e_{(1)}$ can be estimated from Eq. (5.28) as

$$|\chi^e_{(1)}|\sim|\chi^e_0|\frac{\lambda}{|\Delta E_1|}\frac{\langle V_{\text{twist},u}\rangle}{\Delta E_o}, \tag{5.50}$$

with $|\Delta E_1|\equiv E({}^4T_{1g})-E({}^4T_{2g})$, because the electric-dipole moment P becomes nonvanishing only with the aid of odd parity field, i.e., $V_{\text{twist},u}$ in the present problem, as Eqs. (3.3) and (5.27) show, i.e.,

$$|\overline{P}|\sim ea_0\frac{\langle V_{\text{twist},u}\rangle}{\Delta E_o}, \tag{5.51}$$

where a_0 is the Bohr radius. We have assumed as usual that the intermediate state $|j'\rangle$ in Eqs. (3.3) and (5.27) is mainly the $4p$ state of the Cr^{3+} ion so that ΔE_o of Eq. (5.4) $\sim\Delta E(pd)$.

Let us assume the following values for the material constants: $\Delta E(pd)=10$ eV, the spin-orbit coupling constant $\lambda=10$ meV, $\langle V_{\text{twist},g}\rangle\sim\langle V_{\text{twist},u}\rangle\sim 0.1$ eV, $4N=3.3\times10^{28}$ m^{-3}, $|\Delta E_1|\sim 1$ eV, $|\Delta E_2|\sim 2$ eV, the refractive index $n\sim 1$, and the relaxation constant Γ_m in Eq. (5.13) and Eq. (5.28) ~ 0.1 eV.

The relative magnitude of $|\chi^m/\chi^e|$ is then estimated to be of the order of unity:

$$\left|\frac{\chi^m}{\chi^e}\right|\sim\frac{n\mu_B}{cea_0}\frac{\Delta E(pd)}{\langle V_{\text{twist},u}\rangle}\frac{\langle V_{\text{twist},g}\rangle}{\lambda}\frac{|\Delta E_1|}{|\Delta E_2|}\sim 2, \tag{5.52}$$

where we have set the values of the physical constants $\mu_B=e\hbar/2m=9.274\times10^{-24}$ C m^2/s, $c=2.998\times10^8$m/s, $e=1.602\times10^{-19}$ C, and $a_0=0.5292\times10^{-10}m$. This is in good agreement with the observation.[10] The absolute magnitude of $|\chi^e|$ at $2\omega=[E({}^4T_{2g}x_\pm)-E({}^4A_{2g})]/\hbar$ is estimated to be $1\times10^{-12}m/\text{V}$, with $\epsilon_0=8.854\times10^{-12}$ C^2/mJ. This is by one or two orders of magnitude smaller than the value $5\times10^{-11}m/\text{V}$ of $LiNbO_3$ at $\lambda=1.064$ μm.

VI. SPECTRA OF SECOND HARMONICS AND INTERFERENCE EFFECT

In the present coordinate system, the second-order susceptibilities χ^m and χ^e in the point group $\overline{3m}$ have the following symmetries:

$$\chi^m\equiv\chi^{mee}_{xxx}=-\chi^{mee}_{xyy}=-\chi^{mee}_{yxy}=-\chi^{mee}_{yyx}, \tag{6.1}$$

$$\chi^e\equiv\chi^{eee}_{xxx}=-\chi^{eee}_{xyy}=-\chi^{eee}_{yxy}=-\chi^{eee}_{yyx}. \tag{6.2}$$

As a result, the source term for the second harmonics $\boldsymbol{S}$:

$$\boldsymbol{S}=\mu_0\left(\nabla\times\frac{\partial \boldsymbol{M}}{\partial t}+\frac{\partial^2 \boldsymbol{P}}{\partial t^2}\right), \tag{6.3}$$

is expressed as follows:

$$\begin{pmatrix} S_x \\ S_y \\ S_z \end{pmatrix}=\frac{4\omega^2}{c^2}\begin{pmatrix} 2\chi^m E_x E_y-\chi^e(E_x^2-E_y^2) \\ \chi^m(E_x^2-E_y^2)+2\chi^e E_x E_y \\ 0 \end{pmatrix}, \tag{6.4}$$

or

$$\begin{pmatrix} S_+ \\ S_- \\ S_0 \end{pmatrix}=\frac{4\sqrt{2}\omega^2}{c^2}\begin{pmatrix} (-i\chi^m-\chi^e)E_-^2 \\ (i\chi^m-\chi^e)E_+^2 \\ 0 \end{pmatrix}, \tag{6.5}$$

setting $S_\pm=(S_x\mp iS_y)/\sqrt{2}$ and $E_\pm=(E_x\mp iE_y)/\sqrt{2}$, after Fiebig *et al.*[10] From Eq. (6.4) it is clear that the spectra of χ^m and χ^e can be measured separately by observing the second harmonics linearly polarized along x and y axes, respectively, under the irradiation of fundamentals linearly polarized along x or y axis.

Since χ^e is linearly proportional to the magnetization of the sublattice, it is possible to observe the magnetic domains of the antiferromagnetic crystals by using the circularly polarized fundamentals. From Eq. (6.5) the signal intensity $I\propto|\boldsymbol{S}|^2$ for the circularly polarized light is expressed as

$$|\boldsymbol{S}|^2\propto(|\chi^m|^2+|\chi^e|^2)(|E_+|^4+|E_-|^4)-2(\chi_m'\chi_e''-\chi_m''\chi_e')\times(|E_+|^4-|E_-|^4), \tag{6.6}$$

where $\chi^m\equiv\chi_m'+i\chi_m''$ and $\chi^e\equiv\chi_e'+i\chi_e''$. The interference of the second harmonics generated by the magnetic- and electric-dipole moments is described by $\Delta\equiv-2(\chi_m'\chi_e''-\chi_m''\chi_e')$, which is also proportional to the sublattice magnetization, e.g., at the A_1 sublattice. Therefore we can detect the magnetic domains of the crystal through this interference factor Δ by using the circularly polarized light as the pump source. When the magnetic domain to pump is fixed, the total signals of second harmonics show different spectra against positively and negatively circular-polarized fundamentals.

In this section, we draw four spectra of the second-harmonic generation, i.e., $|\chi^m|^2$, $|\chi^e|^2$, and $|\chi(\sigma^\pm)|^2\equiv|\chi^m|^2+|\chi^e|^2\pm\Delta$, using the microscopic expressions of χ^m and χ^e derived in Sec. V.

The energy levels of ${}^4T_{2g}M_s x_m(m=\pm1,0)$ are evaluated by using Eqs. (2.15) and (2.16) with the values estimated from other experiments. The crystalline field splitting $|\Delta E_3|$ (between ${}^4T_{2g}x_0$ and ${}^4T_{2g}x_m$) (Ref. 8) was assumed to be 65 meV, the spin-orbit interaction $\lambda=12$ meV, and the internal magnetic field splitting $\mu_B H_i=25$ meV. The nonmagnetic level of ${}^4T_{2g}x_\pm$, i.e., E_0, is located at $E_0=2.19$ eV. We confine ourselves to sufficiently low temperatures $k_BT\ll\mu_BH_i\simeq300$ K, so that we set the thermal distribution function $\rho_0(M_s)=1$ for $M_s=3/2$ and 0 otherwise at A_1 and A_2 sublattices. From Eqs. (5.13), (5.21), (5.28), and (5.33), it is found that the energy levels relevant to the resonant second-harmonic generations are ${}^4T_{2g}M_s=3/2x_\pm$ and ${}^4T_{2gs}=1/2x_0$. The positions of these energies are estimated from the result of Sec. IV as follows:

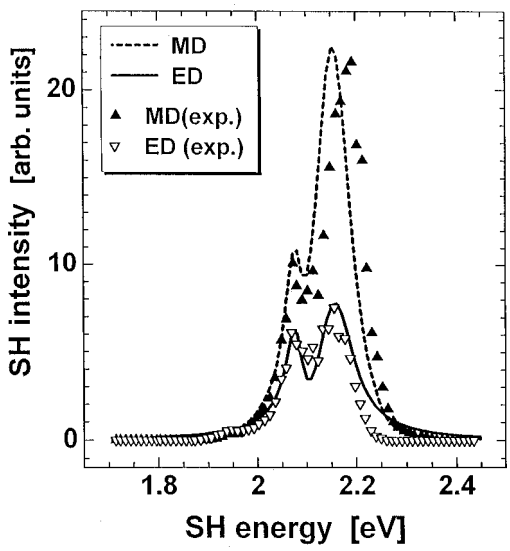

FIG. 4. Calculated spectra of SHG through the magnetic dipole (broken line) and the electric dipole (solid line) as a function of the signal frequency in eV near the transition from ${}^4T_{2g}$ to ${}^4A_{2g}$ at low temperatures.

$$\begin{aligned} &E({}^4T_{2g}M_s=1/2x_0)=2.08\text{ eV},\\ &E({}^4T_{2g}M_s=3/2x_-)=2.14\ 5\text{eV},\\ &E({}^4T_{2g}M_s=3/2x_+)=2.164\text{ eV}. \end{aligned} \tag{6.7}$$

A. Spectra of χ^m and χ^e

In order to compare the observed χ^m and χ^e spectra with the calculated ones, χ^m given by Eq. (5.26) and χ^e given by Eq. (5.47), we introduce several parameters, although we have seen that the most dominant terms are able to explain the observed intensities roughly.

As to the χ^m spectrum, the value of A^m in Eq. (5.13) and the relative magnitude $\chi^m_{(2)}/\chi^m_{(1)}\sim n_{\text{terms}}(3/8)(\lambda/\Delta E_3)^2$ were varied so as to obtain best fitting. Although n_{terms} is supposed to be 12 according to the argument following Eq. (5.25), best fit was found for $n_{\text{terms}}\sim20$. The relaxation rates $\Gamma^m_\pm$ of ${}^4T_{2g}x_\pm$ and Γ^m_0 of ${}^4T_{2g}x_0$ were chosen to be 40 meV and 20 meV, respectively.

The χ^e spectrum was also drawn with the parameters A^e and the ratio $(\chi^e_{(2n)}+\chi^e_{(2)})/\chi^e_{(1)}$. The same values of $\Gamma^e_\pm$ and Γ^e_0 as for χ^m were assumed. Inclusion of $(\chi^e_{(1a)}+\chi^e_{(1b)})$ was also tried to obtain better fit with the observed spectra.

The theoretical spectra of $|\chi^m|^2$ and $|\chi^e|^2$ are shown in Fig. 4. We may say that they reproduce the observed features of the spectra fairly well.

B. Interference effect

The interference effect will be most pronounced when the value of $\Delta\equiv-2(\chi_m'\chi_e''-\chi_m''\chi_e')$ becomes of the same order of magnitude as that of $|\chi^m|^2+|\chi^e|^2$. If we define the phase angles θ_m and θ_e by

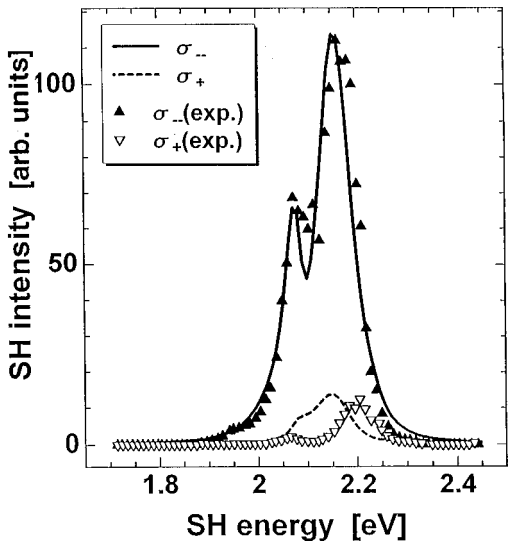

FIG. 5. Calculated second-harmonic signals under σ_- (solid line) and σ_+ (broken line) circularly polarized incoming laser light as a function of the signal frequency in eV. The difference shows the interference effect. The phase of χ^m has been changed by $\pi/2$ rather arbitrarily.

$$\chi^m = |\chi^m| \exp(i\theta_m), \tag{6.8}$$

$$\chi^e = |\chi^e| \exp(i\theta_e), \tag{6.9}$$

we find

$$\Delta = 2|\chi^m||\chi^e| \sin(\theta_m - \theta_e), \tag{6.10}$$

so that the perfect interference will be attained when (1) $|\chi^m| = |\chi^e|$ and (2) $\theta_m - \theta_e = \pm \pi/2$.

From the observed spectra, i.e., Fig. 5(b) of Ref. 10, we find that these conditions are almost satisfied experimentally. Theoretically, we have seen above that the first condition $|\chi^m| \sim |\chi^e|$ is nearly satisfied. However, it is by no means easy to make the second be satisfied near the frequency $\omega_s \equiv 2\omega \simeq [E(^4T_{2g}) - E(^4A_{2g})]/\hbar$. The reasons are that (1) both χ^m and χ^e must be pure imaginary, away from the resonance, as Eqs. (2.30) and (2.31) show, and (2) even in the near resonance region, the phase difference $\theta_m - \theta_e$ will be very small, as long as the relaxation rates $\Gamma^m_\pm, \Gamma^m_0$ are assumed equal or nearly equal to $\Gamma^e_\pm, \Gamma^e_0$. This means that the present theory cannot explain the observed interference quantitatively. If only the phase of χ^m is changed by $\pi/2$ or χ^m multiplied by i for some reason, it will become possible to reproduce the interference fairly well as shown in Fig. 5. Clearly, some effects involving dissipative process must be introduced to modify the expressions of χ^m and/or χ^e in order to overcome this difficulty. As such effects, we can mention the phase changes due to the local field correction[25] and the cross relaxation.[26] However, detailed treatments of them must be left for another paper.

VII. CONCLUSION

The absolute values and the spectra of the ellipticity and polarization rotation observed at the Cr_2O_3 crystal surface have been theoretically well analyzed and explained by our microscopic model. First, we confirmed that only the real part of the product of the magnetic- and electric-dipole matrix elements contributes to the magnetoelectric susceptibility.[19] From this fact, only the conventional trigonal crystalline fields $V_{\text{axial},g}$ and $V_{\text{axial},u}$ are effective in the present phenomena in contrast to the second-harmonic generation[12] in which only $V_{\text{twist},g}$ and $V_{\text{twist},u}$ lead to finite contribution. Second, two levels $|^4T_{2g}x_\mp\rangle$ split by the diagonal component of the spin-orbit interaction contribute with opposite sign to the magnetoelectric susceptibility. This can explain the spectrum structure of ellipticity and rotation at $^4T_{2g}$, i.e., not only the absolute value but also the sign of these signals, very well in contrast to the explanation by Ref. 8. Third, the main spectrum structures at ^2E_g and $^2T_{1g}$ have been well described by the present microscopic model using the material constants determined by other experiments. These transitions are spin forbidden so that the off-diagonal components of the spin-orbit interaction must be involved. Therefore the product of electric- and magnetic-dipole moments is reduced by two orders of magnitude, but this reduction is just compensated by the small relaxation rate of the relevant transitions. As a result, we can explain the large peak signals at ^2E_g and $^2T_{1g}$. The observed intensities of the sidebands at $^2E_g - 1/2u_+$ and $^2T_{1g} - 1/2a_+$ are by one order of magnitude larger than the present model of the static crystalline field but we feel that this discrepancy may be resolved by introducing the dynamical hybridization between $^4T_{2g}x_\pm$ and $^4T_{2g}x_0$ and between $^4T_{1g}a_\pm$ and $^4T_{1g}a_0$. This problem must be left as one of the future problems.

Thus we may conclude that the three important facts in the magnetoelectric spectra observed on the surface of the Cr_2O_3 crystal are well understood by the present microscopic model.

We have derived explicit expressions of the resonance terms of the magnetic and electric susceptibilities which are important for the interpretation of the resonance second-harmonic generation observed by Fiebig *et al.*[10] It was confirmed that the crystalline fields $V_{\text{twist},g}$ and $V_{\text{twist},u}$, together with the spin-orbit interaction $\mathcal{H}_{\text{so}}$, acting on the trigonal states as perturbations, lead to nonvanishing signals of SHG and the interference between χ^m and χ^e below the Néel temperature of Cr_2O_3. Here the judgment of reality of relevant matrix elements has been essential to obtain finite results. We have also seen that the mechanism involving V_{twist} could indeed lead to observed magnitudes of the signal intensity.

It was found that the observed spectra in the region of $^4T_{2g}$ for linearly polarized light could be reproduced fairly well by choosing reasonable values for the adjustable parameters in the theoretical expressions for χ. Apparently, some effects to modify the phases of susceptibilities must be involved. As the two such effects, we suggested in Sec. VI the modification due to the local field correction and the cross relaxation. It was indeed possible to explain the interference by introducing a factor of i for χ^m rather arbitrarily. The origin of this factor offers a very interesting subject for further study. This will be treated in the near future together with the effect of cross relaxation from $|^4T_{2g}3/2x_-\rangle$ to $|^4T_{2g}1/2x_0\rangle$ on χ^e.

ACKNOWLEDGMENTS

This work was supported by a Grant-in-Aid for COE Research on ''Phase Control and Engineering of Spin-Charge-

Photon Coupled Systems'' from The Ministry of Education, Science, Sports and Culture.

APPENDIX: WAVE FUNCTIONS AND REDUCED MATRIX ELEMENTS

In this appendix we first give the wave functions for the three d electrons in the trigonal environment and then derive, using these functions, the expressions for the reduced (or double barred) matrix elements involved in the magnetic and electric susceptibilities, i.e., in Eqs. (5.11) and (5.29). It then turns out that the latter matrix elements are all real, meaning that the nonlinear susceptibilties themselves are purely imaginary in the absence of relaxation as they should be.

The wave functions for the three d electrons of a Cr^{3+} ion in a Cr_2O_3 crystal are derived appropriate to the C_3 symmetry. The ground state of the three d electrons in this crystalline field is expressed by Hund's coupling rule as

$$\Psi({}^4A_{2g}M_s=3/2)=i|x_+x_-x_0|, \tag{A1}$$

$$\Psi({}^4A_{2g}M_s=-3/2)=i|\bar{x}_+\bar{x}_-\bar{x}_0|, \tag{A2}$$

in terms of the Slater determinants describing the state in which the three d electrons occupy the three t_2 states with components ± 1 and 0 of effective angular momentum along the C_3 axis. For the notations and conventions adopted for the wave functions in the C_3 symmetry, the reader is referred to Ref. 15. The up and down spin orbitals for a single electron are represented without and with bars on $x_\pm$ and x_0 orbitals, as in Eqs. (A1) and (A2). The excited electronic states were obtained from the original wave functions given in Ref. 15 by transforming the $t_2(\xi,\eta,\zeta), t_1(\alpha,\beta,\gamma)$, and $e(u,v)$ orbitals in the ordinary cubic coordinate system into $t_2(x_+,x_-,x_0)$, $t_1(a_+,a_-,a_0)$, and $e(u_+,u_-)$ in the present coordinate system whose quantization axis is the C_3 axis. The wave functions obtained in this way are as follows:

$$\Psi({}^4T_{2g}M_s=3/2x_+)=\frac{1}{\sqrt{2}}(|x_+x_-u_+|-|x_-x_0u_-|), \tag{A3}$$

$$\Psi({}^4T_{2g}M_s=3/2x_-)=\frac{1}{\sqrt{2}}(|x_+x_0u_+|-|x_+x_-u_-|), \tag{A4}$$

$$\Psi({}^4T_{2g}M_s=3/2x_0)=\frac{1}{\sqrt{2}}(|x_-x_0u_+|+|x_+x_0u_-|), \tag{A5}$$

$$\Psi({}^4T_{1g}M_s=3/2a_+)=\frac{-i}{\sqrt{2}}(|x_+x_-u_+|+|x_-x_0u_-|), \tag{A6}$$

$$\Psi({}^4T_{1g}M_s=3/2a_-)=\frac{-i}{\sqrt{2}}(|x_+x_0u_+|+|x_+x_-u_-|), \tag{A7}$$

$$\Psi({}^4T_{1g}M_s=3/2a_0)=\frac{-i}{\sqrt{2}}(|x_-x_0u_+|-|x_+x_0u_-|), \tag{A8}$$

$$\Psi({}^2E_gM_s=1/2u_+)=\frac{1}{\sqrt{3}}(-|x_+\bar{x}_+x_-|+|x_+x_0\bar{x}_0| -|x_-\bar{x}_-x_0|), \tag{A9}$$

$$\Psi({}^2E_gM_s=1/2u_-)=\frac{1}{\sqrt{3}}(|x_+\bar{x}_+x_0|-|x_+x_-\bar{x}_-| +|x_-x_0\bar{x}_0|), \tag{A10}$$

$$\Psi({}^2T_{1g}M_s=1/2a_+)=\frac{i}{\sqrt{6}}(-|x_+\bar{x}_+x_-|+|x_+x_0\bar{x}_0| +2|x_-\bar{x}_-x_0|), \tag{A11}$$

$$\Psi({}^2T_{1g}M_s=1/2a_-)=\frac{i}{\sqrt{6}}(|x_+x_-\bar{x}_-|+2|x_+\bar{x}_+x_0| -|x_-x_0\bar{x}_0|), \tag{A12}$$

$$\Psi({}^2T_{1g}M_s=1/2a_0)=\frac{i}{\sqrt{6}}(|\bar{x}_+x_-x_0|+|x_+\bar{x}_-x_0| -2|x_+x_-\bar{x}_0|). \tag{A13}$$

The d orbitals employed here may be expressed as

$$x_+=-(\sqrt{2}d_2^*-d_1)/\sqrt{3}, \tag{A14}$$

$$x_-=(\sqrt{2}d_2-d_1^*)/\sqrt{3}, \tag{A15}$$

$$x_0=d_0, \tag{A16}$$

and

$$u_+=-(d_2^*+\sqrt{2}d_1)/\sqrt{3}, \tag{A17}$$

$$u_-=(d_2+\sqrt{2}d_1^*)/\sqrt{3}, \tag{A18}$$

using the complex orbitals given by

$$d_2=(d_{x^2-y^2}+id_{xy})/\sqrt{2}, \tag{A19}$$

$$d_1=(d_{zx}+id_{yz})/\sqrt{2}, \tag{A20}$$

$$d_0=d_{3z^2-r^2}, \tag{A21}$$

in the present coordinate system.

Let us confirm, before showing that C_m in Eq. (5.11) is real, that the matrix element of $V_{\text{twist},g}$ connecting the states ${}^4T_{2g}M_sx_m$ and ${}^4T_{1g}M_sa_m$ does vanish as long as we remain within the strong field scheme. We can evaluate this matrix element using the three-electron wave functions given above and express it in terms of the one-electron integrals of the crystalline field $v_{\text{twist},g}$ as follows:

$$\langle {}^4T_{2g}M_s x_m|V_{\text{twist},g}[T_1 a_0]|{}^4T_{1g}M_s a_m\rangle$$
$$= \frac{1}{\sqrt{2}}\frac{-i}{\sqrt{2}}(m\langle|x_+x_-u_m||V_{\text{twist},g}||x_+x_-u_m|\rangle$$
$$- m\langle|x_{-m}x_0u_{-m}||V_{\text{twist},g}||x_{-m}x_0u_{-m}|\rangle)$$
$$= \frac{-mi}{2}(\langle x_+|v_{\text{twist},g}|x_+\rangle + \langle x_-|v_{\text{twist},g}|x_-\rangle$$
$$- \langle x_{-m}|v_{\text{twist},g}|x_{-m}\rangle - \langle x_0|v_{\text{twist},g}|x_0\rangle)$$
$$= \frac{-mi}{2}\langle x_m|v_{\text{twist},g}|x_m\rangle. \quad \text{(A22)}$$

It is not difficult to see both $\langle x_\pm|v_{\text{twist},g}|x_\pm\rangle$ vanish, if we express the orbitals $x_\pm$ in terms of the complex and then the real d orbitals with the help of Eqs. (A14) and (A15) and Eqs. (A19) and (A20).

In a similar way, we have

$$\langle {}^4T_{2g}M_s x_0|V_{\text{twist},g}[T_1 a_0]|{}^4A_{2g}M_s\rangle = mi\sqrt{2}\langle u_m|v_{\text{twist},g}|x_m\rangle \quad \text{(A23)}$$

for both $m=+$ and $m=-$ and find that the right hand side is real, which means the reduced matrix element $\langle {}^4T_{2g}\|V_{\text{twist},g}[T_1]\|{}^4A_{2g}\rangle$ is also real according to Eq. (5.10). This time, it will be nonvanishing in general.

For the reduced matrix element appearing in Eq. (5.9), we proceed in the same way:

$$\langle {}^4T_{2g}M_s x_m|P_x^2|{}^4T_{2g}M_s x_0\rangle = -\frac{m}{2}(\langle x_{-m}|p_x^2|x_m\rangle$$
$$+ m\langle x_m|p_x^2|x_0\rangle$$
$$+ \langle u_{-m}|p_x^2|u_m\rangle). \quad \text{(A24)}$$

This result also assures that the matrix element in question is real.

Since the two reduced matrix elements in Eq. (5.11) are found to be real, C_m is real.

We will next show that A^e is real. The reduced matrix element $\langle {}^4T_{1g}\|P_x^2[T_2]\|{}^4A_{2g}\rangle$ is found to be real, because we have

$$\langle {}^4T_{1g}M_s a_m|P_x^2|{}^4A_{2g}M_s\rangle$$
$$= \frac{m}{\sqrt{6}}\langle {}^4T_{1g}M_s a_m|P_x^2[T_2 x_m]|{}^4A_{2g}M_s\rangle$$
$$= -\frac{m}{3\sqrt{2}}\langle {}^4T_{1g}\|P_x^2[T_2]\|{}^4A_{2g}\rangle$$
$$= -\frac{m}{\sqrt{2}}(\langle u_{-m}|p_x^2|x_m\rangle + m\langle u_m|p_x^2|x_0\rangle). \quad \text{(A25)}$$

Now we only have to consider the reality of $\langle {}^4A_{2g}\|\overline{P}_x[T_1]\|{}^4T_{2g}\rangle$. For this purpose, we assume the closure approximation, replacing the two energy denominators in Eqs. (5.27) and (3.3) by some appropriate averages. This then allows us to proceed here also in the same way as before. The left hand side of Eq. (5.30) now can be evaluated as

$$\langle {}^4A_{2g}M_s|\overline{P}_x|{}^4T_{2g}M_s x_m\rangle$$
$$= -i\frac{1}{\sqrt{2}}(m\langle|x_+x_-x_0||\overline{P}_x||x_+x_-u_m|\rangle$$
$$- m\langle|x_+x_-x_0||\overline{P}_x||x_{-m}x_0u_{-m}|\rangle)$$
$$= \frac{-mi}{\sqrt{2}}(\langle x_0|\overline{p}_x|u_m\rangle - m\langle x_m|\overline{p}_x|u_{-m}\rangle). \quad \text{(A26)}$$

We thus find that

$$\langle {}^4A_{2g}M_s|\overline{P}_x|{}^4T_{2g}M_s x_m\rangle = \frac{-m}{6}\langle {}^4A_{2g}||\overline{P}_x[T_1]||{}^4T_{2g}\rangle$$
$$= \frac{-mi}{\sqrt{2}}(\langle x_0|\overline{p}_x|u_m\rangle$$
$$- m\langle x_m|\overline{p}_x|u_{-m}\rangle). \quad \text{(A27)}$$

Using the one-electron orbitals given above, and noting p_x and $V_{\text{twist},u}$ are real, we easily confirm that the reduced matrix element $\langle {}^4A_{2g}\|\overline{P}_x[T_1]\|{}^4T_{2g}\rangle$ is indeed real. This proves the reality of the parameter A^e in Eq. (5.29).

We must next prove the reality of B_n^e. Since $\langle {}^4A_{2g}\|\overline{P}_x[T_1]\|{}^4T_{2g}\rangle$ and $\langle {}^4T_{1g}\|P_x^2[T_2]\|{}^4A_{2g}\rangle$ have already been proved to be real, it only remains to see the reality of $\langle {}^4A_{2g}\|\overline{P}_x[T_2]\|{}^4T_{1g}\rangle$.

The left hand side of Eq. (5.35) is obtained as

$$\langle {}^4A_{2g}M_s|\overline{P}_x|{}^4T_{1g}M_s a_m\rangle = \frac{-1}{\sqrt{2}}(\langle x_0|\overline{p}_x|u_m\rangle$$
$$+ m\langle x_m|\overline{p}_x|u_{-m}\rangle). \quad \text{(A28)}$$

Arguing in the same way as before, we find the reduced matrix element $\langle {}^4A_{2g}\|\overline{P}_x[T_2]\|{}^4T_{1g}\rangle$ to be real, which implies that B_n^e in Eq. (5.38) is real. It will be needless to say that B^e is also real.

Finally, we give below the expression of the matrix elements which are necessary to verify the reality of C_a^e in Eq. (5.43) and C_b^e in Eq. (5.45):

$$\langle {}^4T_{2g}M_s x_m|V_{\text{trig}}^c|{}^4T_{1g}M_s a_m\rangle = -\frac{mi}{\sqrt{6}}\langle {}^4T_{2g}\|V[T_{2g}]\|{}^4T_{2g}\rangle$$
$$= -\frac{3mi}{2}\langle x_m|v_{\text{trig}}^c|x_m\rangle, \quad \text{(A29)}$$

and

$$\langle {}^4A_{2g}M_s|\overline{P}_x^c|{}^4T_{1g}M_s a_m\rangle = \frac{m}{6}\langle {}^4A_{2g}\|\overline{P}_x^c[T_2]\|{}^4T_{1g}\rangle$$
$$= \frac{-1}{\sqrt{2}}(\langle x_0|\overline{p}_x^c|u_m\rangle$$
$$+ m\langle x_m|\overline{p}_x^c|u_{-m}\rangle). \quad \text{(A30)}$$

The relevant reduced matrix elements are all real.

[1] See, e.g., *Optical properties and Electronic Structure of Metals and Alloys*, edited by F. Abeles (North-Holland, Amsterdam, 1965).
[2] See references in the paper by P. S. Pershan, J. Appl. Phys. **38**, 1482 (1967).
[3] G. S. Canright and A. G. Rojo, Phys. Rev. B **46**, 14 078 (1992); Phys. Rev. Lett. **68**, 1601 (1992).
[4] I. E. Dzyaloshinskii, Phys. Lett. A **155**, 62 (1991).
[5] S. Spielman, J. S. Dodge, L. W. Lombardo, C. B. Eom, M. M. Fejer, T. H. Geballe, and A. Kapitulnik, Phys. Rev. Lett. **68**, 3472 (1992), and references therein.
[6] A. L. Shelankov and G. E. Pikus, Phys. Rev. B **46**, 3326 (1992).
[7] B. B. Krichevtsov, V. V. Pavlov, R. V. Pisarev, and V. N. Gridnev, J. Phys.: Condens. Matter **5**, 8233 (1993).
[8] B. B. Krichevtsov, V. V. Pavlov, R. V. Pisarev, and V. N. Gridnev, Phys. Rev. Lett. **76**, 4628 (1996). The trigonal splitting here is larger than the one assumed by D. S. McClure (Ref. 13).
[9] M. Fiebig, D. Fröhlich, G. Sluyterman v.L., and R. V. Pisarev, Appl. Phys. Lett. **66**, 2906 (1993).
[10] M. Fiebig, D. Fröhlich, B. B. Krichevtsov, and R. V. Pisarev, Phys. Rev. Lett. **73**, 2127 (1994).
[11] V. N. Muthukumar, R. Valenti, and C. Gros, Phys. Rev. Lett. **75**, 2766 (1995); Phys. Rev. B **54**, 433 (1996).
[12] Y. Tanabe, M. Muto, and E. Hanamura, Solid State Commun. **102**, 643 (1997).
[13] D. S. McClure, J. Chem. Phys. **38**, 2289 (1963).
[14] S. Sugano and Y. Tanabe, J. Phys. Soc. Jpn. **13**, 880 (1958).
[15] S. Sugano, Y. Tanabe, and H. Kamimura, *Multiplets of Transition-Metal Ions in Crystals* (Academic, New York, 1970).
[16] See, however, M. Shinada, S. Sugano, and K. Kushida, J. Phys. Soc. Jpn. **21**, 217 (1966).
[17] For the notations and use of irreducible tensor operators, see, e.g., Ref. 15. See also J. S. Griffith, *The Irreducible Tensor Method for Molecular Symmetry Groups* (Prentice-Hall, Englewood Cliffs, NJ, 1962); and P. H. Butler, *Point Group Symmetry Applications: Methods and Tables* (Plenum, New York, 1981).
[18] The $^4T_{1g}$ state considered here belongs to the electron configuration t^2e.
[19] R. M. Hornreich and S. Shtrikman, Phys. Rev. **171**, 1065 (1968).
[20] Y. Tanabe, Prog. Theor. Phys. Suppl. **14**, 17 (1960).
[21] T. Iizuka-Sakano and E. Hanamura, J. Phys. Soc. Jpn. **67**, 332 (1998).
[22] J. W. Allen, R. M. Macfarlane, and R. L. White, Phys. Rev. **179**, 523 (1969).
[23] R. M. Macfarlane and J. W. Allen, Phys. Rev. B **4**, 3054 (1971).
[24] M. Inoue and Y. Toyozawa, J. Phys. Soc. Jpn. **20**, 363 (1965).
[25] R. W. Boyd, *Nonlinear Optics* (Academic, New York, 1992).
[26] L. J. Rothberg and N. Bloembergen, Phys. Rev. A **30**, 820 (1984).